Mouse germline cysts contain a fusome that mediates oocyte development

Madhulika Pathak[1] and Allan C. Spradling[1,2]

[1]Howard Hughes Medical Institute Research Laboratories

Carnegie Institution for Science, Baltimore, MD 21218, USA

[2]Lead contact, to whom correspondence should be addressed

ABSTRACT

Mouse female primordial germ cells (PGCs) undergo five synchronous, incomplete mitotic divisions, and send each resulting germline cyst into meiosis to fragment and produce 4-6 oocytes and 24-26 supportive nurse cells. However, no system of polarity has been found to specify mammalian oocytes, link them appropriately to nurse cells and enable them to acquire high quality organelles and cytoplasm. We report that mouse cysts develop an asymmetric Golgi, endoplasmic reticulum (ER) and microtubule-associated "fusome", similar to the oocyte-determining fusome in Drosophila cysts. The mouse fusome distributes asymmetrically among cyst cells and enriches in future oocytes with Pard3, and Golgi-endosomal UPR (unfolded protein response) proteins. Spindle remnants rich in stable acetylated microtubules, like those building the Drosophila and Xenopus fusomes, transiently link early mouse cyst cells for part of each cell cycle. A non-random gap in these microtubules predicts that initial cysts fragment into similar six-cell derivatives, providing a potential mechanism for producing uniform oocytes. Together with previous studies these results argue that a polarized fusome underlies the development of female gametes from the PGC to follicular oocyte stages in diverse animals including mammals.

INTRODUCTION

Early female germ cell development occurs within interconnected cysts formed by consecutive incomplete divisions of a germline stem cell (GSC) or primordial germ cell (PGC) in diverse animals. These include basal species like hydra (Littlefield, 1994), nematodes like C. elegans, insects like Drosophila, and vertebrates including fish, frogs, mice and humans (Gondos, 1973; King, 1970; Lin et al. 1994; Pepling and Spradling, 1998; Kloc et al. 2004; Marlow and Mullins, 2008; review, Spradling, 2024). As they develop, Drosophila and other insect cyst cells become interconnected by ring canals and acquire polarity associated with a microtubule-rich "fusome" (Giardina, 1901; King, 1970; Lin et al. 1994; Büning, 1994; Huynh and St Johnston, 2004). In Drosophila, the fusome arises from mitotic spindle remnants generated during

incomplete cytokinesis, contains ER cisternae and displays Par gene and microtubule-dependent polarity that is essential for oocyte production. Later, in meiotic prophase, the fusome mediates the movement of centrioles, mitochondria, and germ plasm regulators such as oskar mRNA into the oocyte where they form the Balbiani body (Bb) (Mahowald and Strassheim, 1970; Cox and Spradling, 2003). Remarkably, mammalian oocytes undergo these same events (review: Spradling et al. 2022), but a fusome has not been detected, raising the possibility that mammalian cyst polarity and oocyte specification use a different system.

Studies in Xenopus long provided suggestions that cyst polarization in at least some vertebrate species resemble the invertebrate process (Kloc et al. 2004; review: Huynh and St Johnston, 2004). Recently a detailed study using modern methods characterized fusome-containing Xenopus cysts sharing many such similarities including production of relatively few oocytes and mostly nurse cells (Davidian and Spradling, 2025). Here, we report new studies on mouse cyst polarization. In the mouse, germ cells are induced around embryonic day 6.5 (E6.5) (Lawson et al. 1999) and begin migrating toward the gonad as PGCs. En route, PGCs start to reprogram their epigenetic state to pluripotency (Seki et al. 2007; Saitou et al. 2011; Loda et al. 2022; Liu et al. 2025). After they enter the gonad at E10.5, PGCs take on germ cell character (Nicholls et al. 2019), turn on DDX4 and initiate cyst formation while reprogramming is still ongoing. During E11.5 they induce Dazl, a major post-transcriptional mediator of early germ cell development, pluripotency re-establishment, and meiotic entry (Ruggiu et al. 1997; Haston et al. 2009; Gill et al. 2011; reviewed in Fu et al. 2015; Zagore et al. 2018; Yang et al. 2020). Even before meiotic entry, Dazl is needed to form stable cysts in zebrafish (Bertho et al. 2021) and in mice (Rosario et al. 2019).

The formation of germline cysts in mice is more complicated than in most animals. Mouse germline cysts arise from five rounds of mitotic divisions beginning at E10.5, so that each PGC generates almost 32 cells. However, the cysts break variably into an average of 4.8 smaller cysts before these divisions are completed at E14.5 when cells enter meiosis (Lei and Spradling, 2013; Levy et al. 2024). During meiosis,

each smaller cyst slowly loses component cells, as every 2 days about one cell on average becomes activated to act as a nurse cell. The nurse cell transfers most of its cytoplasm into the residual cyst, shrinks to a small remnant and undergoes programmed cell death (Lei et al. 2016; Niu and Spradling, 2022; Ikami et al 2023). In the pachytene substage of meiosis I, there is a substantial reorganization that brings mitochondria and ER sheets into close proximity by E18.5 (Ruby et al,. 1969; Nogawa et al. 1988; Pepling and Spradling, 2001). Cyst breakdown is complete by 5 days after birth (P5) with the formation of 4-6 primordial follicles, each containing a single oocyte in which organelles largely transferred from nurse cells are gathered into an aggregate known as the Balbiani body (Niu and Spradling, 2022). Cyst polarity guides cyst fragmentation and oocyte specification, polarization and organelle acquisition. Despite this, the only prior hint of a mouse fusome was a round structure that could be stained with certain antisera in PGCs and 2-cell cysts (Hahnel and Eddy, 1987; Pepling and Spradling, 1998).

Germline cysts also support germ cell rejuvenation, the universal process that allows damage to be removed each generation so that species can persist without known limit. Germline rejuvenation takes place during meiosis in single celled eukaryotes (Unal et al. 2011; Suda et al. 2024; Xiao and Unal, 2025). Processes that rejuvenate organelles such as mitochondria, restore rDNA copy number, and reset epigenetic chromatin marks have also been documented in meiosis during animal gametogenesis (Cox and Spradling, 2003; Hill et al. 2014; Reik and Surani, 2015; Bohnert and Kenyon, 2017; Lieber et al. 2019, Pang et al. 2023; Yamashita, 2023;Xiao and Unal, 2025; Spradling et al. 2025). The Balbiani body in newly formed oocytes is associated with germ plasm formation and selection for mitochondrial function in many species (Heasman et al. 1984; Kloc et al. 2004b; Marlow and Mullins, 2008; Spradling et al. 2022; Sekula et al. 2024). Currently, however, germline rejuvenation events are thought to skew toward late oogenesis (Bohnert and Kenyon, 2017; Xiao and Unal, 2025).

Here we report that mouse PGCs and cyst cells elaborate a fusome-like structure that is rich in Golgi, endosomal vesicles and ER associations. The mouse fusome distributes asymmetrically with stable

microtubules that persist for part of the cell cycle. By the 8-cell stage, cyst cells reorganize into a rosette configuration that brings cells with multiple bridges (potential oocytes) and associated fusome material closer together. Developing cysts at this stage usually fragment non-randomly at sites lacking microtubule connections into six-cell cysts, implying that mouse ovarian cyst structure is more highly controlled than previously realized (Lei and Spradling, 2013; Levy et al. 2024). Beginning as PGCs and throughout cyst formation, endosome-Golgi associated degradation (EGAD)-mediated UPR pathway proteins including Xbp1 are expressed, suggesting that the oocyte proteome quality control begins very early and continues. After pachytene, centrosome/Golgi-rich elements move to the oocyte and mediate the acquisition of organelles by the Bb. These results imply that a polarized fusome whose properties have been significantly conserved in diverse animals including mammals underlies female gamete development from the PGC to follicular oocyte stages.

RESULTS

PGCs contain a Golgi-rich structure known as the EMA granule

Early observations of a germ cell "(e)mbryonic (m)ouse (a)ntigen (EMA)" (Hahnel and Eddy, 1987) identified an "EMA granule" in mouse primordial germ cells that resembles the Drosophila spectrosome, a fusome precursor (Lin et al. 1994; Pepling et al. 1998). To investigate this relationship further, we determined that the EMA granule appears in PGCs as early as E9.5 and continues to be expressed in later cysts (Figure 1A, Figure S1A). We used lineage labeling to mark cysts (Video S1B) derived from single PGCs, and 3D surface rendering and volume quantification (Figure S1C), to demonstrate a significantly uneven distribution of the EMA granule within PGC daughter cells (Figure 1B). This asymmetry and studies described below prompted us to name the EMA-rich structure the "mouse fusome".

The EMA-rich material reorganized and clustered together in female cysts by E13.5 (Figure 1C; Video S1D1-2; Figure S1E), whereas in male cysts it remained separate and similar-sized in each cell (Figure 1C' and graph; Figure S1E') reminiscent of male differences in the Drosophila fusome (Diegmiller et al. 2023). In females, cyst regions with enriched fusome staining contained an average of 3 Tex14-positive bridges, whereas unenriched zones had an average of just 1 (Figure 1D-D' graph; Figure S1F). Thus, highly branched cells with more bridges, which are known to give rise to most oocytes (Lei and Spradling, 2013; Lei and Spradling, 2016; Ikami et al. 2023), contain more fusome. Similar clustering, known as rosette formation (Figure 1H), and increased fusome accumulation in pro-oocytes, characteristically occur as germline cysts grow in Drosophila and other species (see Hegner, 1914; Büning, 1994; Huynh and St Johnston, 2004). Rosette formation is thought to prepare for sharing between nurse cells and oocytes.

The mouse fusome is enriched in Golgi elements and vesicles

The fusome co-stained with the Golgi protein Gm130 (Figure 1F, Figure S1H) and the recycling endosomal protein Rab11a1 (Figure 1F'). Electron microscopy (EM) of mouse germ cells showed a prominent Golgi and endocytic vesicles in most E11.5 and E12.5 cyst germ cells in a subregion of similar

shape to the EMA granule in light micrographs. (Figure 1E'; Figure S1K-L) consistent with a previous EM observation (Jeon and Kennedy, 1973). We found evidence that EMA granules require ongoing Golgi activity to be maintained. In E11.5 mouse ovaries cultured in vitro, treatment with the Golgi-inhibitor Brefeldin A for 6 hours caused EMA granules to shrink, but many reformed within 18h of its removal (Videos S1I1-3). The fusome often partly overlaps with ER (Figure S1K-K'). EM sections of E14.5 cysts revealed clusters of Golgi within adjacent cyst cells near ring canals as expected for cysts after rosette formation (Figure 1E, 1E"). EMA-1 antisera react with multiple fucosylated glycolipids (Apostolopoulos et al. 2015; Figure S1J). EMA staining disappears from germ cells at E14.5 (Figure 1I), however, very similar (but non-germ cell-specific) staining is also seen with wheat germ agglutinin (WGA) (Figure 1G) and this staining continues at E13.5 and later stages (Figure 1G'; Figure S1G) .

The mouse fusome overlaps centrosomes and associates with microtubules

A cell's microtubule cytoskeleton emanates from its centrosomes and from non-centrosomal microtubule organizing centers (ncMTOCs); it frequently controls trafficking of Golgi elements and positions them near centrosomes. To investigate whether the fusome associated with microtubules, we stained E11.5 gonads with anti-acetylated tubulin (AcTub) and EMA. The fusome overlapped the centrosomes in interphase germ cells (Figure 2A), indicating it usually occupies a peri-centriolar domain. In germ cells undergoing mitosis (Figure 2B), the fusome associated with centrioles during interphase, but (typical for Golgi) dispersed as the mitotic spindle forms and for most of metaphase. In telophase, fusome vesicles gather at the spindle poles in both daughter cells and at the arrested cytokinesis furrow, which still retains the elongated spindle/midbody microtubules typical of cyst-forming cell cycles (Figure 2B). Small EMA-positive vesicles often associated with these telophase spindles, providing evidence that fusome vesicles can move along microtubules (Figure 2C, Figure S2E). 3D summary movies of germ cells at each mitotic stage stained for AcTub and EMA are shown in Figure S2A.

The mouse fusome was rarely seen at just one pole of a mitotic spindle, like the Drosophila fusome at early stages of GSC and cystoblast division (de Cuevas and Spradling, 1998). Some EMA-reactive material appears at the cytokinesis furrow before it is seen at the fusome (Figure 2C; Figure S2C-D). Asymmetry in the mouse fusome distribution arose only in late telophase. Clusters of fusome and centrosomes approached the arrested furrow (Figure 2D, S2C-D). At this point short microtubule arrays were visible (Figure S2C). Small fusome-containing vesicles are often observed in association with microtubules as shown in Figure S2E. Soon after, the amount of fusome in the two daughter cells becomes asymmetric, suggesting that differential activity or persistence of fusome transport late in cytokinesis generates asymmetry. Ovaries cultured briefly in vitro support continued germ cell division and fusome asymmetry. Fusome formation is severely affected in such cultures if microtubules (MTs) are disrupted by cold or by Ciliobrevin D treatment (Figure S2F graph).

Cyst fragmentation is non-random and correlates with microtubule gaps

Mouse cysts produce an average of 4-6 oocytes per PGC as a result of initial cyst breakage into multiple, independently developing subcysts that each produce one oocyte (Lei and Spradling, 2013; Niu and Spradling, 2022). Production of uniform-sized oocytes, as observed, would seem to require programmed breakage into uniform subcysts (Spradling et al. 2022), but some random breakage also occurs (Lei and Spradling, 2013; Ikami et al. 2023; Levy et al. 2024). To assess a role of microtubules and the fusome in programming cyst fragmentation, we tracked AcTub and the fusome in lineage-labeled E12.5 cysts. In about 10% of interphase cysts, presumably those in very late telophase or early in the subsequent cell cycle, persistent microtubule arrays were observed that connected the cells in pairs (Figure 2E). When we examined a total of about 50 large cysts, 15 larger cysts of 7-10 cells were found where the MTs in all cells could be analyzed completely. Three examples are shown in which projections of 8-cell lineage-labeled cysts are outlined (dashed lines). In the left column, lineage, the fusome and MTs are shown (Fig. 2E-E"; Figure S2H). Unexpectedly, the microtubule connections (middle column) showed a large

discontinuity of 10μ or more between just two of the cystocytes (Figure 2E). Likewise, microtubule bundles in E' and E" are also absent between two cells (straight dashed line Figure 2E'-E" and Figure S2H'). The absence of an MT connection predicts cyst breakage, as observed in one of the cysts (Figure 2E"), where separation into a 2-cell and 6-cell cyst has already occurred. We also examined how the fusome distributes in these cysts (Figure S2H').

The patterns of cyst breakage predicted by MT absence were highly non-random (Figure 2F). A 6-cell cyst is predicted based on the position of the microtubule gaps in 13/15 8-cell to 10-cell cysts analyzed: see Figure 2E, Figure S2H (movies of an 8-cell (upper), or 10-cell cyst (lower), with cleavage diagram); and Figure S2H' (fusome separation in the 3 cysts from Fig. E-E"). A binomial probability calculation showed that the chance of obtaining a 6-cell cyst product in 13 of 15 trials following random breakage of a single junction in an 8-cell cyst (where 2 of 7 broken linkages produce a 6-cell product) was at most 4.53E-06.

The mouse fusome associates with polarity and microtubule genes including Pard3

Microtubules play a critical role in ovarian cyst formation and polarity in multiple species. Some of the most important regulators of MTs and polarity are the Par proteins that function in epithelial cell polarity, embryonic development, asymmetric neuroblast division (Petronczki and Knoblich, 2001; Hapak et al. 2018) and oocyte formation in C. elegans, Drosophila and vertebrates (Kemphues et al. 1988; Huynh and St Johnston, 2004; Moore and Zernicka-Goetz, 2005). Drosophila meiotic cysts express Par3/Baz and Par6, another apical Par complex protein, along with beta-catenin/Arm in a ring-like arrangement close to the ring canals (Cox et al. 2001; Huynh et al. 2001a, 2001b; Huynh and St Johnston, 2004). This relatively small membrane zone likely represents the apical domain of cyst germ cells.

We investigated the expression of Pard3, the mouse ortholog of Par3/Baz to determine if a similar arrangement of the highly conserved Par proteins occurs in mouse germline cysts. Pard3 expression localized around the fusome but extended beyond it, a pattern reminiscent of the larger ring of Baz in Drosophila cyst cells (Figure 3A, Figure S3A). At E13.5, cysts in rosette configuration show Pard3 and the

fusome enriched around a central cell (Figure 3B, dashed region from Video S3B1) but not in E13.5 male cysts (Video S3B2). This co-localization was validated in multiple lineage-labeled E13.5 cysts (Figure 3D; Figure S3D and S3E). Ring canals were concentrated in this zone (Figure 3C and Figure S3C), hence mouse cysts have ring canals and an apical Par protein in the same small anterior location as in Drosophila, and that mouse fusome occupies the corresponding zone as the Drosophila fusome. These findings suggest that mammals form and polarize oocytes using a conserved system found in diverse animals based on Par genes, cyst formation and a fusome.

The mouse fusome associates with Golgi genes involved in UPR beginning at the onset of cyst formation

We performed single cell RNA sequencing (scRNA seq) of mouse gonads to gather additional fetal germ cell data (see Methods) and combined them with data from Niu and Spradling (2022) to make an integrated dataset of more than 3,000 germ cells spanning E10.5 to P5 (Figure 3F-H; Figure S3F-I). Our gene expression studies showed that PGCs and early cysts actively express many genes that enhance proteome quality by monitoring, refolding or expelling misfolded or aggregated proteins for degradation. The Unfolded Protein Response (UPR) pathway associated largely with the ER in yeast is regulated by Hac1, the ortholog of Xbp1. We observed high levels of Xbp1 (Figure 3I) and many of its target genes (Figure 3I and I') that increase quality secretory protein production. Membrane proteins and lipids are also promoted by this pathway.

In animals the UPR pathway has been expanded with several additional branches (Mitra & Ryoo, 2019, Sicari, 2019) . We also observed expression Creb3l2 (ER/Golgi resident transcription factor), ATF4 (General UPR transcription factor activated by Golgi stress), Golph3 (Golgi phosphoprotein for membrane trafficking) and Arfgap(s) (involved in both Golgi to ER-and Golgi to endosome trafficking) during mouse cyst formation (Figure S3J). Xbp1 activates genes such as the chaperones (Hsp5a/Bip, Hsp90b1;DNAjc10; Lman2; Dnajb9), protein-disulfide isomerases (Erp44, Pdia3, Pdia4, Pdia6, Creld2), the Endoplasmic Reticulum Associated Degradation (ERAD) regulator Syvn1/Hrd1 and the ERAD components (Sec61b;

Ubxn4, Psmc6, Ube2j2, Get4, Ufd1) (Taniguchi and Yoshida, 2017). Thus, repair and expansion of ER, Golgi and secretory components begins immediately or even before migrating PGCs reach the gonad (Figure 3I).

Xbp1 also supports synthesis of ER membrane phospholipids via upregulation of targets such as Elovl1, Elovl5, and Elovl6, and Chka, Other highly expressed targets maintain ER and Golgi structure and are orthologs of Drosophila fusome proteins (Figure 3I', Lighthouse et al., 2008). Thus the adaptive UPR pathway and its branches are active during cyst formation, and later in prophase as well (Figure 3I-3I').

UPR genes are active during cyst formation and depend on Dazl.

We investigated how cyst development and fusome formation depend on Dazl. First, we confirmed that Dazl$^{-/-}$ mice retard the PGC to germ cell transition (Figure S4C-E). Dazl$^{-/-}$ E12.5 cysts showed higher levels of the DNA methylase Dnmt3a expression compared to controls (Figure 4A; Figure S4B) suggesting that germ cell DNA demethylation has slowed. Ring canals highlighted by staining for Tex14 were only half the size of wild type canals at E13.5 or structurally abnormal showing that cyst formation was slowed and cytokinesis was sometimes abnormal (Figure 4B).

We also performed scRNA sequencing of Dazl female homozygous mutant gonads at E11.5 and E12.5 and re-clustered them with wild type germ cells at these stages for comparison (Figure 4C). At E11.5 the merged germ cells cluster together suggesting that Dazl$^{-/-}$ has minimal effects on germ cells at E11.5, the stage it is first expressed (Figure 4C). However, E12.5 WT and Dazl$^{-/-}$ germ cells cluster separately (Figure 4C). Wild type and Dazl$^{-/-}$ expressed similar amounts of EGAD mediated UPR pathway genes at E11.5 germ cells (Figure S4F) whereas wild type germ cells expressed lower levels compared to Dazl$^{-/-}$ cells at E12.5 (Figure 4C'). Thus, UPR genes in Dazl$^{-/-}$ cells act similarly to pluripotency genes, and retain higher expression levels at E12.5 than wild type.

The high expression of Xbp1 and many of its target genes in PGCs and early cyst cells argues that early germ cells are expanding ER and Golgi production and increasing membrane protein quality. To

validate that XBP1 is active in germ cells, we employed an IRE1-XBP1 ratiometric assay which utilizes a genetically encoded dual-fluorescent reporter system (see Methods, Figure S4I). First, we performed magnetic-activated cell sorting (MACS) to purify SSEA1 labelled germ cells from the E11.5 gonad (Figure S4G-H). We delivered the IRE1-XBP1 sensor to SSEA1+ve germ cells and SSEA1-ve control somatic cells by transfection. Both types of cells fluoresce in proportion to IRE1-splicing activity which measures Xbp1activation activity. The construct also constitutively expresses a fluorescent marker such that the color ratio will represent a quantitative measure of relative IRE1-XBP1 activity between cells and under different conditions. Our observations showed that IRE1-Xbp1 activity in E11.5 germ cells was significantly higher than in somatic cells (Figure 4D; Figure S4I). Dazl mutant cells showed persistent higher levels of Xbp1 activity at E12.5 (Figure 4D'-4D''').

The adaptive UPR pathway destroys misfolded proteins using proteasome activity, particularly the 20S proteasome (Vember and Brodsky, 2008; Figure 4H). We measured proteasome activity within E11.5 PGCs to investigate whether the UPR pathway was paired with increased proteasome activity indicating it served an adaptive cellular mechanism of cell rejuvenation in PGCs destined to produce oocytes. Using a fluorogenic substrate to measure 20S Proteasome activity, we compared MACS sorted germ cells to somatic cells and found that germ cells have significantly higher proteasome activity than somatic cells at E11.5 (Figure 4E) and E12.5 (4E' Left). Proteasome activity continued to stay even higher in E12.5 Dazl-/- germ cells suggesting stressful persistent activation of UPR keeping Dazl-/- germ cell in an arrested state (Figure 4E' Right, 4E").

We also studied the effects of Dazl mutation on the asymmetric enrichment of fusome in cells with multiple ring canals. Using both EMA and a Golgi marker, Gs28, we observed that germ cell Golgi begins to fragment in *Dazl*$^{-/-}$ mutant germ cells even by E12.5 (Figure 4F, dotted circles, graph). High levels of Golgi stress documented by the increased IRE1-Xbp1 activity, and elevated proteolysis in these cells, may lead to such fragmentation. These problems were accompanied by a dramatic arrest in cyst polarity

development. *Dazl*$^{-/-}$ germ cells at E13.5 showed virtually no differential expression of Pard3 or enrichment of fusome within particular cyst cells (Figure 4F'). Finally, in *Dazl*$^{-/-}$ P0 gonads, large cells destined by become oocytes do not appear (Video S5E3, Video S5F3). The effects of Dazl-/- on germline cyst development and meiosis are summarized in Figure 4G. These observations collectively indicate an essential function of the mouse fusome in temporal regulation of the EGAD-UPR pathway within germ cells (Figure 4H). The observed loss of polarity caused by Dazl-/- mutation can explain the failure of oocyte production and the sterility of Dazl homozygotes.

The mouse fusome is associated with organelle rejuvenation during meiosis

In Drosophila, starting at pachytene the microtubule cytoskeleton changes its structure, and polarity (Cox and Sprading, 2006). The new polarity, with microtubules running along the fusome such that minus ends cluster in the oocyte, prepares selected nurse cell organelles for transport into the oocyte and the Bb of a new primordial follicle. Mouse nurse cell centrosomes, mitochondria, Golgi, ER and possibly other organelles also move from nurse cells to the oocyte between P0 and P4 in a microtubule-dependent process (Lei and Spradling, 2016; Niu and Spradling, 2022). Prior to or during these events, Drosophila mitochondria are selected and rejuvenated by programmed mitophagy to enhance functionality (Cox and Spradling, 2003; Lieber et al. 2019; Palozzi et al. 2022; Monteiro et al. 2023). It is not currently known if selection and rejuvenation take place before movement to the oocyte, or if a significant amount also takes place en route.

Because the fusome is directly involved in organelle movement to the Drosophila Balbiani body we looked for changes in the fusome and in gene expression that might relate to organelle rejuvenation and movement to the oocyte. For the reasons explained previously (see text for Figure 1G) we used WGA as fusome marker beyond stage E14.5. Fusome staining with WGA persists within meiotic germ cells at E17.5 (Figure 5A; Figure S5A-B). Fusome volume remained in proportion with germ cell ring canal number, as outer nurse cells (with one ring canal) transfer organelles and cytoplasm to cells with more ring canals

located closer to oocytes (Figure 5A, graph; Video S5C). Pard3 content also showed such a proportion (Figure 5A' graph). At E18.5, cyst development in the medulla toward wave 1 follicles, diverged from wave 2 follicles in the cortex that become quiescent primordial follicles (Figure 5B) (Yin and Spradling, 2025). Wave 1 oocytes grow substantially in volume, fusome and Pard3 content due to cytoplasmic transfer from surrounding nurse cells which decrease in size (Figure 5B-B', graph. Video S5E1, Video S5F1). Oocyte enrichment of the fusome and Pard3 was confirmed using lineage labelled cysts at P0 (Figure 5C and 5D). Such enrichment was significantly reduced in Dazl+/- heterozygotes (Figure 5E graph, Video S5E2, Video S5F2).

Wave 2 follicles which produce nearly all fertile oocytes, increase organelle content beginning at E18.5 and contain a finished Bb by P4 (Niu and Spradling, 2022). Initially, 4-5 transfered Golgi-centrosome pairs were observed at separate cytoplasmic locations in oocytes. These gradually come together and form an oval-shaped cytocentrum that nucleates a microtubule aster and organizes the Balbiani body. We carried out immunofluorescent staining at E18.5 and examined EMs that documented interactions between Golgi, ER and mitochondria. Figures 5F-F' show a wild type germ cell with a large crescent of perinuclear mitochondria (AT5a) adjacent to a large cluster of fusome (WGA). An EM provides a higher resolution view of a similar interaction (Figure 5F'). In contrast, relatively few mitochondria or fusome were stained in a Dazl+/- heterozygote (Figure 5F"). Mitochondria also interact extensively with ER at this time (Figure 5G; Pepling et al. 2007). ER tracker and Mitotracker (Figure 5G') stained clusters throughout much of the germ cell cytoplasm.

DISCUSSION

Mouse germline cysts contain a fusome

One of the earliest and most highly conserved steps in animal gamete development is the formation of polarized germline cysts (Giardina, 1901; Wilson, 1925; Büning, 1994; Matova and Cooley, 2001; Lu et al. 2017; Gerhold et al. 2022; Sprading et al. 2022). In the ovaries of most species, cysts become polarized

during the synchronous mitotic cycles whose incomplete cytokinesis connects daughters via characteristic ring canals. In Drosophila, germline cyst divisions also produce and asymmetrically distribute a microtubule and vesicle-rich fusome whose polarity is essential to specify oocytes in addition to nurse cells. We found that mouse germline cysts also contain a similar organelle, the "mouse fusome." As in Drosophila, the mouse fusome starts as a small, membrane-rich cytoplasmic region within migrating PGCs before they arrive at the gonad. The nascent organelle propagates asymmetrically during synchronous, incomplete cyst divisions, involving stabilized spindle microtubules rich in AcTub and a program of arrested cytokinesis that produces distinctive ring canals. Stainable fusome MTs persist for only part of each cell cycle, but polarity is maintained since over five successive mitotic cycles the cyst undergoes rosette formation, predicts cleavage into smaller cysts and concentrates fusome material in future oocytes. Finally, the mouse fusome associates in a distinctive manner with the apical Par complex located near the clustered ring canals, as originally described for the fusome in Drosophila cysts (Cox et al. 2001; Huynh et al. 2001a, 2001b). Apical-basal patterning of Drosophila oocytes differs from many epithelial cells (review Huynh and St Johnston, 2004), but our studies show that both mouse and Drosophila oocytes localize the fusome and ring canals in a similar relationship to the apical Par domain.

How conserved are fusomes in distant animal groups?

The recent detailed analyses of fusomes in Xenopus (Davidian and Spradling, 2025) and here in mice, provide an opportunity to compare fusomes over a wider range of animals than was possible when well characterized fusomes were limited to Holometabolous insects. Based on these examples, the most highly conserved aspects of polarized cyst production are the cell cycle changes that arrest telophase, stabilize the midbody and lead to incomplete cytokinesis (Gerhold et al. 2022; Price et al. 2023). Somehow this process polarizes the microtubules that arise in the fusome segment within the nascent ring canal, and becomes a building block in growing cyst polarity. A longstanding mystery regarding fusome microtubule polarity is its exceptionally high sensitivity to microtubule inhibitors like colchicine, which appears to be

much greater than cell division generally, or other developmental processes requiring microtubue-dependent vesicle transport (Koch and Spitzer, 1983). The sensitivity continues later in meiosis, since treating E17.5 mouse ovary cultures with just 10 nM colchicine strongly reduced Balbiani body formation, but had no measurable effect on cell division (Lei and Spradling, 2016). Interestingly, mouse cysts develop asymmetry during a later period in cytokinesis than Drosophila cysts (Figure 2C-D). In Xenopus, another fusome-related property, cyst-wide divisional synchrony, showed more variation between sister cells than in tightly coordinated Drosophila cyst cells (Davidian and Spradling, 2025).

Qualitative differences in fusome structure and behavior have evolved between major animal groups. Drosophila fusomes and those of related insects are stabilized by an essential, proteinaceous skeleton containing alpha-spectrin, tropomodulin and germline-specific isoforms of adducin-like proteins generated by differential splicing and cleavage of a polyprotein precursor produced by the Hts gene (Petrella et al. 2007). This skeleton may have evolved to control access to the fusome and hence to the oocyte by intracellular parasites such as Wolbachia bacteria. An alpha-spectrin-containing skeleton was not detected in Xenopus fusomes (Davidian and Spradling, 2025) or in these experiments in mouse. The Xenopus fusome has robust microtubules, that may independently control access. This structural difference may explain earlier failures to identify fusomes in vertebrates using orthologs to Drosophila fusome proteins like alpha-spectrin.

Association of the mouse fusome with Golgi

The major role apparently played by Golgi in the mouse compared to the Drosophila or Xenopus fusomes is potentially significant. In contrast, the Drosophila fusome contains abundant ER cisternae, whose presence may facilitate lipid biosynthesis needed to produce high levels of new plasma and organellar membranes. Not does rapid cyst formation demand high amounts of fresh membranes, but rejuvenation of new germ cells may require that their lipids and proteins be newly synthesized from simple building blocks (see Spradling et al. 2025). Mouse cysts grow more slowly, and may associate extensively

with Golgi because of an early high demand for protein secretion. In mouse, the zona pellucida directly contacts the oocyte and begins to be produced and secreted by the oocyte in primary follicle oocytes have just begun to develop. In contrast, the analogous Drosophila egg coating, the vitelline membrane, is produced by somatic follicle cells, and only starting in more mature follicles. Even primordial follicles oocytes contain abundant Golgi and multivesicular bodies near the Balbiani body (Niu and Spradling, 2022). Thus, fusome's apparently stronger association with the Golgi in mouse but with the ER in Drosophila probably just reflects differences the relative relative timing and speed of events in oogenesis that take place in both organisms. This highlights the need to study fusome behavior throughout oogenesis and in the context of ongoing developmental and rejuvenation activity.

Mouse cysts develop multiple uniform oocytes using a novel specific-cleavage mechanism

Mouse PGCs generate 4-6 oocytes using a multi-step mechanism involving synchronous incomplete cyst divisions, limited fragmentation into smaller cysts (involving <10% of cell-cell junctions) and continuous, slow nurse cell turnover (Lei and Spradling, 2013; Lei and Spradling, 2016; Niu and Spradling, 2022. Despite their complex pathway, mouse oocytes in newly formed primordial follicles appear quite uniform in size and are efficiently produced (Spradling, 2022), suggesting that a majority develop from final cysts of similar size and nurse cell content. However, lineage analyses showed many cyst cells move apart apart at least transiently. Live imaging studies revealed active movements likely responsible for cell displacement, as well as some cell detachment caused by random breakage (Levy et al. 2024).

Our studies of mouse fusome microtubules indicated that oocyte uniformity is promoted by programmed cyst breakage during mitotic divisions into cysts of uniform size (Figure 2G). AcTub arrays in cysts of 7-10 cells frequently contained a single large gap lacking MTs between a group of 6-cells, and the other residual cells. Such gaps in a major cytoskeletal element of germ cells subjected to significant tissue movements would likely become breakage sites (Figure 2E"). Previous experiments also supported a special role for 6-cell cysts. We conclude that germline cyst breakage is largely programmed and efficient 6-cell

cyst production explains the high frequency of synchronous six-cell mitoses observed during E11.5-E13.5 (Pepling and Spradling, 1998 and directly mapped 6-cell cysts in young cyst stages prior to E14.5 (Lei and Spradling, 2013). Efficient cell turnover and transfer of most nurse cell contents into the oocyte probably explains the 5.1-fold increase in Golgi, 4.9-fold increase in mitochondria and 5-fold increase in the number of accumulated centrosomes measured in P4 oocytes compared to E14.5 germ cells (Lei and Spradling, 2016).

How might growing cysts be programmed to acquire a gap in remnant spindle microtubule bundles affecting a specific junction? One possibility is the uneven distribution of the fusome in four cell cysts (Figure 1B"). If the fusome is involved in stabilizing and associating with spindle remnants, shortly after M phase, the cell with the lowest fusome amount might fail acquire a spindle remnant of the necessary size at the next division, leading to 6:2 breakage. Involvement of the microtubule cytoskeleton in asymmetric divisions has been observed in many other situations (Fichelson & Huynh, 2007; Kaltschmidt & Brand, 2002; Sunchu & Cabernard, 2020; Meiring et al., 2020; Planelles-Herrero et al., 2022; Watson et al., 2023). Significantly, other sources of variation likely also occur at a lower level. Synchronously dividing 8-cell and 16-cell cysts are readily detected in low numbers (Pepling and Spradling, 1998). These large cysts may represent a specific alternative pathway, that may preferentially take place in cysts within one of the three follicle waves that occur in mouse (Niu and Spradling, 2025). The model in Figure 2G, also predicts production of 4 2-cell cysts which were commonly observe in prior to E14.5 and the onset of substantial nurse cell transfer (Lei and Spradling, 2013, Supplement).

Dazl regulates cyst formation, fusome polarization, and oocyte specification

Female gamete development in many organisms is extensively controlled at the post-trancriptional level by RNA binding proteins (Mercer et al 2021; Conti and Kunitomi, 2024). In vertebrates, the RNA-binding protein Dazl is widely conserved and controls multiple aspects of early germ cell development by regulating a large number of target transcripts (Zagore et al. 2018). In mice, Dazl modulates the ongoing

reprogramming of new arrived gonadal PGCs to pleuripotency beginning at E11.5 when it turns on (Gill et al. 2011; Nicholls et al. 2019, Haston et al. 2009). Normally, Dazl continues to function at later stages of oocyte development (Conti and Kunitomi, 2024), but Dazl mutants fail to enter or progress in meiosis.

Our studies defined a series of new functions for Dazl during cyst formation. We confirmed that pluripotency reactivation is slowed in Dazl mutants since DNA demethylation was delayed, and pluripotency genes failed to start downregulating at E12.5. Homozygous Dazl mutant females failed to normally regulate UPR genes, leaving their mRNA levels elevated. This likely resulted from a failure to downregulate their Xbp1 activator, since both Xbp1 activity and 20S proteosome activity was also elevated in Dazl-/- germ cells. Overactivation of the UPR pathway appeared to cause Golgi fragmentation. These effects resembled the general slowing of normal developmental progression, as with pleuripotency downregulation. We also observed abnormal cyst formation with some small and defective ring canals as in zebrafish Dazl mutants (Bertho et al. 2021), but cysts remained intact and continued to develop. This allowed us to document that Dazl is needed for cysts and their fusomes to become polarized. In Dazl mutants, cysts did not undergo rosette formation or concentrate the fusome or Pard3 in cells with multiple ring canals. Oocytes apparently could not be specified and did not form. These results show that Dazl acts as a regulator that is essential for the many important aspects of cyst formation and oocyte production.

Germ cell rejuvenation is highly active during cyst formation

Germ cells have long been known to propagate species without know limits over evolutionary time by rejuvenating gametes each generation in association with meiosis (Weissmann, 1892; Kirkwood, 1987). Recently, the detailed cellular and molecular genetic mechanisms that make this possible both in single-celled eukaryotes and in animals have generated increasing interest (Cox and Spradling, 2003; Unal et al., 2011; Chen et al. 2014; Bohnert and Kenyon, 2017; Lieber et al., 2019; Palozzi et al., 2022; Spradling et al., 2022; Yamashita, 2023; Xiao and Unal, 2025). By studying the fusome, which is already present in migrating PGCs and E9.5, and by sequencing mouse germ cells from the earliest stages of ovarian

development beginning at E10.5, we gained new insights into the timing and processes that likely contribute to germ cell rejuvenation during mouse oogenesis.

These studies made it clear that multiple rejuvenation mechanisms are highly active from the earliest times of germ cell development (Figure 3I). In animals the UPR pathway has been modified by the addition of several additional pathways besides the Ire1-Xba1 branch, all of which were expressed in early germ cells. Creb3l2 controls a transcription factor that increases production COPII vesicles that carry out ER to Golgi transport and maintain a balance between secretory supply and demand. Insufficient matching can lead to Golgi stress (Machemer, 2015), which can be managed by activating the ATF4 pathway branch.

Expression of Xbp1mRNA or even Xbp1 protein using a general antibody is not sufficient to show Xbp1 activity, since this is controlled by Ire1-mediated splicing to produce the active Xbp1s isoform. We were able to purify enough E11.5 and E12.5 germ cells to carry out biochemical assays and show that mouse female germ cells have substantial levels of Xbp1s activity at both times, higher than in somatic cells. The high expression of many known Xbp1 targets also documents the high activity of this pathway (Figure 3I,I'). Early germ cells also express genes suggesting that they are expanding membranes via lipid biosynthesis and secretory pathway activity. Consistent with active adaptive-UPR rejuvenation of their proteomes we documented substantial levels of active proteolysis in early germ cells at both E11.5 and E12.5

The observations reported here suggest that EGAD—an emerging proteostatic mechanism plays a previously unappreciated role. EGAD complements the well-established ERAD pathway by facilitating the clearance of misfolded proteins via Golgi-endosome trafficking and proteolysis, rather than removal from the ER and degradation in the proteosome as in ERAD. We observed substantial amounts of ERAD based on the expression of Xbp1 and its many targets, and its documented activity and its endpoint 20S proteosome activity. It is hard to quantitatively compare the amount of EGAD activity, but the prominent role Golgi throughout the stages of mouse oogenesis and its location at the core of the Balbiani body

suggests that EGAD either fulfills a unique role in oocyte production. or else is uniquely capable of operating at the highest level of proteostatic activity demanded by the much greater challenge of germline rejuvenation compared to any other tissue without generating damaging and self-limiting side effects.

Rejuvenation genes were also highly expressed later in meiosis during zygotene and pachytene, in diplotene when mitochondria/ER contact is extremely high (Figure 5G), as well as in primordial follicles (Figure 3I,I' "Dc"). The early appearance of the fusome and its association with Golgi and ER-related processes that are central to adaptive-UPR, suggests that in animals, rejuvenation begins earlier in the generational cycle than it does in single celled eukaryotes. Animal germ cells return to a pleuripotent state by the end of cyst formation. Cyst formation precede meiosis and represents an opportunity to enhance the rejuvenation process (Spradling et al. 2025). Our findings of early rejuvenation activity align with those of Palozzi et al. (2022), who showed that mitochondrial rejuvenation during oogenesis uses a special germline mitophagy and begins at the onset of meiosis. In yeast, mouse and C. elegans oocytes, damaged materials are destroyed by lysosome-like degradation in mature oocytes and at meiosis II (Bohnert and Kenyon, 2017; Zaffagnini et al. 2024; Xiao and Unal, 2025), similar to the lysosome-like turnover of remnant nurse cells, and residual fusome contents near the onset of follicle formation in mouse and Drosophila. Thus, animal oocytes may engage in rejuvenation activities from before meiosis begins until meiosis II is completed.

In sum, our experiments argue that mouse germline cysts are produced by an ancient conserved process that modulates spindle microtubules to generate an asymmetric polarized fusome associated with apical Par proteins that enrich in oocytes. Proteins and processes involved in cellular rejuvenation are highly active throughout meiotic prophase and begin even in migrating PGCs. Germline cyst polarity ensures that organelles gathered from the nurse cells are delivered to the oocyte where they form a Balbiani body. In Drosophila, germline cysts, fusomes and Par-mediated polarity are all essential for oocyte production. The parallels shown here across 500 million years of evolution strengthen the case that germline

cysts and polarized fusomes are likely to have been maintained in evolution because they contribute to the existential task of rejuvenating germ cells each generation,

SUPPLEMENTAL INFORMATION

Supplementary Figures: S1 – S5

Supplementary Videos: S1A, S1B, S1D1, S1D2, S1I1-S1I3, S2A1, S2A2, S2A3, S2A4, S2A5, S2H1, S2H2, S3A, S3B1, S3B2, S5C, S5D, S5E1-E3, S5F1-F3 can be found here: https://drive.google.com/drive/folders/1XuOoesa_WKMJUaVTpOKGbWWhn_fJc56M

ACKNOWLEDGEMENTS

We thank Wanbao Niu and Mike Sepanski for generating a laboratory archive of EM images of mouse ovaries that was used to prepare Figures 1E and 5H. We thank Wanbao Niu, Qi Yin, and Ashish Tiwari for sharing insights on mouse developmental genetic technology and its application to the ovary. The authors thank Ru-ching Hsia for assistance in electron microscopy including the images of Figures 1E' and S1K. We thank Dr. Eugenia Dikovsky for skillfully managing the Carnegie mouse facility. We thank Allison Pinder and Dr. Feric Tan for assistance with genomics. We thank members of the Spradling lab for helpful comments throughout the course of the research and publication process. Allan Spradling is a Staff Member of the Carnegie Institution for Science who hosts the laboratory at its former Department of Embryology and provides generous additional support.

DECLARATION OF INTERESTS

We declare no competing financial interests. One of us (ACS) is an adjunct professor (without compensation) at the Johns Hopkins University Department of Biology and Johns Hopkins University School of Medicine.

FIGURE LEGENDS

Figure 1. Mouse pre-meiotic PGCs contain a "fusome."

A. PGCs and early germline cysts from E9.5-E12.5 ovaries. EMA (red), DAPI (blue). Boxed regions magnified at right (R) (arrows, EMA granules). B. EMA granule asymmetry in a 2-cell E11.5 cyst: Yellow cells represent a lineage-labelled 2-cell cyst marked with both YFP (green, lineage) and DDX4 (red). B′. Boxed region showing EMA granules (white triangles). Graph at R: EMA granule volumes consistently differ between daughter cells in 2-cell cysts. N=16. B″. Varying volumes of daughter cells within E12.5 4-cell lineage-labeled cysts. EMA granules (white triangles), EMA (red). Graph at R: EMA volume asymmetry, N=18; C. Rosette formation in E13.5 ovary and E13.5 testis (C'). GCNA (nuclei, green), EMA (fusome, red; outline, dotted white). Graph at R: % of female (blue) and male (red) cysts with branched fusomes indicative of rosette formation (N=26 for each). D. Ring canal enrichment in high-fusome cells. A E13.5 lineage-labeled (YFP, green) cyst, fusome (EMA, red; outline, dotted white), and ring canals (TEX14, yellow). D' Zoomed image (boxed region in D) showing branched region with enriched fusome (white triangle) containing multiple ring canals. Graph at R: Ring canal number vs. fusome enrichment (≥10 μm^3). N=54. E-E″. EM of an E14.5 cyst in rosette configuration showing a Golgi-rich fusome spanning an intercellular bridge (E''). E'. EM of an E11.5 PGC with a Golgi-enriched region (red outline) and likely EMA granule (compare to 1A-B). F-F'. E11.5 germ cells with EMA granules (EMA, red) co-stained with the Golgi markers F. (GM130, green) or F' (Rab11a1, green). G. Co-staining of WGA (red) and EMA (green) in E11.5 germ cells. G'. WGA (red) staining of rosette fusome in E13.5 ovary: GCNA (nuclei, green). (H) Schematic of rosette formation in 4-cell cyst. (I) Plot showing EMA staining loss in germ cells after E13.5. (N=15 per stage). Student's t-test was used for each graph in Figure 1. (*** = $p<0.001$). Scale bars: 5µm (A, F, F′), 10µm (B-B″, C-C′, D′, G-G′), 20µm (D), 2µm (E).

Figure 2. Stabilized spindle microtubules mediate fusome asymmetry and cyst breakage.

A. Pericentric fusome localization in E11.5 germ cells. The early fusome (EMA granule) associates with centrosomes (dashed arrowheads) in E11.5 germ cells: EMA (red), centrosomes PCNT (Pericentrin, green). Left column shows PCNT and DAPI alone. A′. Summary. B. Fusome (EMA) behavior during indicated stages of the 1st cyst cell cycle. B'. Diagrams summarize behavior at the listed mitotic stages deduced by AcTub staining. C, C'. Symmetric early telophase fusome. D,D'. Asymmetric fusome segregation during late cytokinesis. B-D. EMA, acetylated tubulin (Ac. Tub) and DAPI. E-E''. Three lineage-marked (YFP) E12.5 8-cell cysts (E-E'') in early interphase stained to reveal microtubules (AcTub) and fusome (EMA). The absence of spindle remnants in one cyst region (gap in AcTub) predicts future cyst breakage (blue dashed line, summary at R only of YFP+ cells). The E'' cyst has already broken into 2-cell and 6-cell cyst derivatives. F. Frequency distribution predicted cyst breakage products by size based on 15 lineage-labeled cysts analyzed as in E (7-cell: 3; 8-cell: 8; 9-cell:1; 10-cell:3). Binomial test (see text) compared observed 6-cell cyst production frequency (13/15) to prediction for single random junction breakage of an 8-cell cyst). (****$p<0.0001$). G. Model of cyst production and breakage into four 6-cell cysts and 4 2-cell cysts. Scale bars: 5µm (B), 10µm (A, C-E).

Figure 3. Mouse fusome associates with Pard3 and apical polarity

A-B. Pard3 associates with fusome at E11.5-E13.5 (A, A') and after rosette formation at E13.5 (B, B'). C-C'. Ring canals (RACGAP) localize within the Pard3+ apical domain. D. A lineage-labeled E13.5 cyst (YFP); channels below show enrichment of Pard3 with enriched fusome. Graph: Quantification of Pard3 stained area colocalizing with large->=20 μm^2 and small <20 μm^2 fusome within lineage labelled cyst (Student's t-test, N=13; ***$p<0.001$). E. Xbp1 enrichment in EMA granule of E11.5 PGC. F-H. scRNAseq of E10.5-P5 gonad. UMAP of re-clustered germ cells at various stages (F), UMI (G) NC =nurse cells. (H): UMAP with clusters labelled in ascending order of meiotic development. pre-meiotic (Pre-M), leptotene (Lp), zygotene (Zy), pachytene (Pa), diplotene (Dp), dictyate (Dc). (I-I′) Bar plots: I. Xbp1, Xbp1-target expression plots. I.' Genes orthologous to fusome components. Scale bars: 10µm (A-C), 20µm (D).

Figure 4. UPR genes are active during cyst formation and controlled by Dazl

(A) Dnmt3a and EMA levels at E12.5. Dnmt3a levels are reduced in WT compared to Dazl$^{-/-}$ germ cells. Graph- Dnmt3a fluorescent levels within germ cells as normalized with somatic cells in WT versus Dazl mutant gonad. (N=10 tissues; **p<0.05). (B) Ring canals are smaller and defective in E13.5 Dazl$^{-/-}$ cysts compared to WT. (N=44; **p<0.05). (C) scRNA seq of E11.5 and E12.5 WT and Dazl -/- gonad germ cells. UMAP. Germ cell clusters overlapped at E11.5 and segregated at E12 of WT and Dazl$^{-/-}$. (C') Xbp1, Xbp1 targets, and fusome orthologs in WT vs Dazl$^{-/-}$ germ cells. (D) Validation of IRE1-Xbp1 assay: Ovarian cells visualized by fluorescent microscopy showing GCNA labelled bigger germ cells with higher Xbp1 fluorescence than smaller somatic cells (D'-D"') IRE1-Xbp1 assay comparing SSEA1+ germ vs SSEA1− somatic cells at E11.5 and WT vs Dazl$^{-/-}$ germ cells at E12.5. (D'; 6 experiments: ~32 mice, ≥5 mice and >=20 ovaries per experiment, D"-D"'; 3 experiments: ~40 mice, ≥5 mice and >=25 ovaries per experiments, *p<0.05, **p<0.01, ***p<0.005, ****p<0.0001) (E-E″) Proteasome activity comparing SSEA1+ germ vs SSEA1− somatic cells at E11.5 and WT vs Dazl$^{-/-}$ germ cells at E12.5. (N=3 biological assays with ~35–60 E11.5 ovary per assay and ~25–28 E12.5 ovaries were used per assay. *p<0.05, **p<0.01, ***p<0.005, ****p<0.0001) (F) Golgi fragmentation in E12.5 Dazl$^{-/-}$ germ cells. Graph: germ cell percent with fragmented Golgi in wildtype versus Dazl mutant mouse gonad (Student's t-test: N=16, ***p<0.005) (F') Failure of E13.5 Dazl$^{-/-}$ germ cells to form EMA rosettes or enrich Pard3. G. Dazl$^{-/-}$ effects on fusome, Golgi and Pard3. H. Proposed function of fusome mediated regulation of ERAD-UPR proteostasis. Scale bar: 10μm (except zoomed in 2μm).

Figure 5. Fusome and Pard3 Associate with ER and mitochondria prior to Balbiani body formation

A. E17.5 ovary stained for WGA, GCNA, and TEX14. A'. E17.5 ovary stained for GCNA, RACGAP and PARD3; Graph: Fusome volume and Pard3 Stained area versus ring canal number (N=65 (Fusome volume; N=51 (Pard3); ANOVA, ***p<0.005, ****p<0.0001). B-B′. E18.5 ovary shows WGA-Fusome/Pard3 enrichment in large medullary oocytes vs smaller nurse cells; line: medulla/cortex boundary; dotted circle:

large medullary oocytes; white dotted area: small nurse cells. Area marked as white dotted rectangle is shown as zoomed inset (white arrow). Black arrow in inset: WGA stained fusome; Graph compares fusome volume and Pard3 stained area versus Germ cell nucleus diameter (N=54 (WGA), N=37(PARD3); Student's paired t-test, *p<0.05, ****p<0.001). C. Single cell lineage labelled E18.5 ovary stained for YFP, DAPI, WGA and GCNA Graph: Within single-cell lineage-labeled E18.5 ovary-Fusome volume difference according to germ cell nucleus size (N=10; ****p<0.0001). D. Single cell lineage labelled E18.5 ovary stained for YFP, PARD3 and GCNA Graph: Within single-cell lineage-labeled E18.5 ovary- difference in PARD3 stained area according to germ cell nucleus size (N=10; ***p<0.005). G-G′. Dazl+/- E18.5 ovary-Fusome (WGA) and Pard3 enrichment failure in medullary Oocytes (GCNA). Graph: Fusome volume in potential Oocytes i.e., bigger germ cells with nucleus diameter d>=12 µm in Wildtype versus Dazl +/- mutant F-F″. Organelle enrichment analysis: E18.5 (WT-F-F', and Dazl+/- ovary-F") stained for WGA, mitochondrial marker ATP5a and GCNA (F and F"). F' -EM image of Golgi-rich Fusome (arrow) surrounded by mitochondria. G-G′. ER-mitochondria association in E18.5 WT ovary: G-EM image of ER tubules (arrow) wrapping mitochondria and G'- E18.5 WT ovary- GCNA, ER and Mitochondria tracker staining. Scale bars: 20µm (A-E, G-G′, F,F", G′), 5µm (B-, B′- righ most inset panel), 0.5µm (EM images F′, G).

REFERENCES

Apostolopoulos, V., Stojanovska, L., & Gargosky, S. E. (2015). MUC1 (CD227): A multi-tasked molecule. Cellular and Molecular Life Sciences, 72, 4475-4500. DOI: https://doi.org/10.1007/S00018-015-2014-Z

Adam Bohnert, K., & Kenyon, C. (2017). A lysosomal switch triggers proteostasis renewal in the immortal C. elegans germ lineage. Nature. *551:7682*, *551*(7682), 629-633. DOI: https://doi.org/10.1038/nature24620

Anderson, E., & Beams, H. W. (1960). Cytological observations on the fine structure of the guinea pig ovary with special reference to the oogonium, primary oocyte and associated follicle cells. Journal of Ultrastructure Research, 3, 432-446. https://doi.org/10.1016/S0022-5320(60)90021-6.

Bertho, S., Clapp, M., Banisch, T. U., Bandemer, J., Raz, E., & Marlow, F. L. (2021). Zebrafish dazl regulates cystogenesis and germline stem cell specification during the primordial germ cell to germline stem cell transition. Development, 148. DOI: https://doi.org/10.1242/DEV.187773

Bohnert, K.A., Kenyon, C., 2017. A lysosomal switch triggers proteostasis renewal in the immortal C. elegans germ lineage. Nature 551, 629–633. https://doi.org/10.1038/ nature24620.

Büning J. (1994). The Insect Ovary: Ultrastructure, Previtellogenic Growth and Evolution. Chapman and Hall. DOI: https://doi.org/10.1007/978-94-011-0741-9

Chen, H. H., Welling, M., Bloch, D. B., Muñoz, J., Mientjes, E., Chen, X., Tramp, C., Wu, J., Yabuuchi, A., Chou, Y. F., Buecker, C., Krainer, A., Willemsen, R., Heck, A. J., & Geijsen, N. (2014). DAZL Limits Pluripotency, Differentiation, and Apoptosis in Developing Primordial Germ Cells. Stem Cell Reports, 3, 892. DOI: https://doi.org/10.1016/J.STEMCR.2014.09.003

Clark, J. M., & Eddy, E. M. (1975). Fine structural observations on the origin and associations of primordial germ cells of the mouse. Developmental Biology, 47, 136-155. https://doi.org/10.1016/0012-1606(75)90269-9.

Conti M, Kunitomi C. (2024). A genome-wide perspective of the maternal mRNA translation program during oocyte development. Semin Cell Dev Biol. 154(Pt B), 88-98. doi: 10.1016/j.semcdb.2023.03.003.

Cox, D. N., Seyfried, S. A., Jan, L. Y., & Jan, Y. N. (2001). Bazooka and atypical protein kinase C are required to regulate oocyte differentiation in the Drosophila ovary. Proceedings of the National Academy of Sciences of the United States of America, 98, 14475-14480. DOI: https://doi.org/10.1073/pnas.261565198

Cox, R. T., & Spradling, A. C. (2003). A Balbiani body and the fusome mediate mitochondrial inheritance duringDrosophila oogenesis. Development, 130, 1579-1590. DOI: https://doi.org/10.1242/DEV.00365

Cox, R. T., & Spradling, A. C. (2006). Milton controls the early acquisition of mitochondria by Drosophila oocytes. Development, *133*, 3371-3377. https://doi.org/10.1242/DEV.02514

de Cuevas, M., & Spradling, A. C. (1998). Morphogenesis of the Drosophila fusome and its implications for oocyte specification. Development, 125, 2781-2789. https://doi.org/10.1242/DEV.125.15.2781

Davidian A, and Spradling AC (2025). Early female germline development in Xenopus laevis: stem cells, nurse cells and germline cysts. Proc. Natl. Acad. Sci. USA 122, e2522343122. doi: 10.1073/pnas.2522343122.

Diegmiller R, Imran Alsous J, Li D, Yamashita YM, Shvartsman SY. (2023). Fusome topology and inheritance during insect gametogenesis. PLoS Comput Biol. 19, e1010875. doi: 10.1371/journal.pcbi.1010875.

Fazel, A. R., Schulte, B. A., & Spicer, S. S. (1990). Glycoconjugate unique to migrating primordial germ cells differs with genera. The Anatomical Record, 228, 177-184. DOI: https://doi.org/10.1002/AR.1092280209.

Fazel, A. R., Schulte, B. A., Thompson, R. P., & Spicer, S. S. (1987). Presence of a unique glycoconjugate on the surface of rat primordial germ cells during migration. Cell Differentiation, 21 199-211. DOI: https://doi.org/10.1016/0045-6039(87)90456-8

Fichelson, P., & Huynh, J. R. (2007). Asymmetric Divisions of Germline Cells. Progress in Molecular and Subcellular Biology, 45, 97-120. https://doi.org/10.1007/978-3-540-69161-7_5.

Fu, X. F., Cheng, S. F., Wang, L. Q., Yin, S., de Felici, M., & Shen, W. (2015). DAZ Family Proteins, Key Players for Germ Cell Development. *International Journal of Biological Sciences*, *11*(10), 1226. https://doi.org/10.7150/IJBS.11536.

Gerhold, A. R., Labbé, J. C. and Singh, R. (2022). Uncoupling cell division and cytokinesis during germline development in metazoans. *Front. Cell Dev. Biol.* 10, 1–16.

Giardina AG (1901). Origine dell'oocite e delle cellule nutrici nel Dytiscus. Internationale Monatsschrift Fur Anatomie Und Physiologie, 18, 417-484.

Gill, M. E., Hu, Y. C., Lin, Y., & Page, D. C. (2011). Licensing of gametogenesis, dependent on RNA binding protein DAZL, as a gateway to sexual differentiation of fetal germ cells. Proc. Natl. Acad. Sci.108, 7443-7448. https://doi.org/10.1073/pnas.1104501108

Ginsburg, M., Snow, M. H. L., & Mclaren, A. (1990). Primordial germ cells in the mouse embryo during gastrulation. Development, 110, 521-528. DOI: https://doi.org/10.1242/DEV.110.2.521

Gondos, B. (1973). Intercellular Bridges and Mammalian Germ Cell Differentiation. Differentiation 1, 177-182. https://doi.org/10.1111/J.1432-0436.1973.TB00112.X

Hahnel, A. C., & Eddy, E. M. (1987). The distribution of two cell surface determinants of mouse embryonal carcinoma and early embryonic cells. Journal of Reproductive Immunology 10, 89-110. https://doi.org/10.1016/0165-0378(87)90069-6.

Hapak SM, Rothlin CV, Ghosh S. (2018). PAR3-PAR6-atypical PKC polarity complex proteins in neuronal polarization. Cellular and Molcular Life Sciences. 75, 2735-61.

Haston, K. M., Tung, J. Y., & Reijo Pera, R. A. (2009). Dazl Functions in Maintenance of Pluripotency and Genetic and Epigenetic Programs of Differentiation in Mouse Primordial Germ Cells In Vivo and In Vitro. PLOS ONE 4, e5654. https://doi.org/10.1371/JOURNAL.PONE.0005654

Heasman, J., Quarmby, J., & Wylie, C. C. (1984). The mitochondrial cloud of Xenopus oocytes: The source of germinal granule material. Developmental Biology, *105*(2), 458-469. https://doi.org/10.1016/0012-1606(84)90303-8

Hegner, R. W. (1914). Studies on germ cells. I. The history of the germ cells in insects with special reference to the Keimbahn-determinants. II. The origin and significance of the Keimbahn-determinants in animals. Journal of Morphology, 25, 375-509. DOI: https://doi.org/10.1002/JMOR.1050250302

Hen, G., Friedman-Einat, M., & Sela-Donenfeld, D. (2014). Primordial germ cells in the dorsal mesentery of the chicken embryo demonstrate left-right asymmetry and polarized distribution of the EMA1 epitope. Journal of Anatomy, 224, 556-563. https://doi.org/10.1111/JOA.12163.

Hill, J. H., Chen, Z. & Xu, H. (2014) Selective propagation of functional mitochondrial DNA during oogenesis restricts the transmission of a deleterious mitochondrial variant. Nat. Genet. 46, 389-392.

Hinnant, T. D., Merkle, J. A., & Ables, E. T. (2020). Coordinating Proliferation, Polarity, and Cell Fate in the Drosophila Female Germline. Frontiers in Cell and Developmental Biology 8, 19. DOI: https://doi.org/10.3389/FCELL.2020.00019.

Huynh, J.-R., Petronczki, M., Knoblich, J.A., and St Johnston, D. (2001a). Bazooka and PAR-6 are required with PAR-1 for the maintenance of oocyte fate in *Drosophila.* Curr. Biol. *11*, 901–906.

Huynh, J. R., Shulman, J. M., Benton, R., & St Johnston, D. (2001b). PAR-1 is required for the maintenance of oocyte fate in Drosophila. Development, 128, 1201-1209. https://doi.org/10.1242/DEV.128.7.1201

Huynh JR, St Johnston D. (2004). The origin of asymmetry: early polarisation of the Drosophila germline cyst and oocyte. Curr Biol. 14, R438-49. doi: 10.1016/j.cub.2004.05.040.

Ikami, K., Shoffner-Beck, S., Weh, M. T., Schnell, S., Yoshida, S., Miranda, E. A. D., Ko, S., & Lei, L. (2023). Branched germline cysts and female-specific cyst fragmentation facilitate oocyte determination in mice. Proceedings of the National Academy of Sciences of the United States of America, 120. https://doi.org/10.1073/PNAS.2219683120

Jeon, K. W., & Kennedy, J. R. (1973). The primordial germ cells in early mouse embryos: Light and electron microscopic studies. Developmental Biology. 31, 275-284. https://doi.org/10.1016/0012-1606(73)90264-9

Jung, J. G., Kim, D. K., Park, T. S., Lee, S. D., Lim, J. M., & Han, J. Y. (2005). Development of Novel Markers for the Characterization of Chicken Primordial Germ Cells. STEM CELLS 23, 689-698. https://doi.org/10.1634/STEMCELLS.2004-0208

Kaltschmidt, J. A., & Brand, A. H. (2002). Asymmetric cell division: microtubule dynamics and spindle asymmetry. Journal of Cell Science, 115, 2257-2264. DOI: https://doi.org/10.1242/JCS.115.11.2257

Kemphues, K. J., Priess, J. R., Morton, D. G., & Cheng, N. (1988). Identification of genes required for cytoplasmic localization in early C. elegans embryos. Cell, 52, 311-320. DOI: https://doi.org/10.1016/S0092-8674(88)80024-2.

Kirkwood, T.B. (1987). Immortality of the germ-line versus disposability of the soma. Basic Life Sci. 42, 209–218. https://doi.org/10.1007/978-1-4613-1939-9_15, 1987.

Koch EA, Spitzer EH (1983). Multiple effects of colchicine on oogenesis in Drosophila: Induced sterility and switch of potential oocyte to nurse-cell developmental pathway. Cell Tissue Res 228, 21-32

King RC. (1970). Oogenesis in Drosophila melanogaster. Academic Press: New York.

Kloc M, Bilinski S, Dougherty MT, Brey EM, Etkin LD. (2004a). Formation, architecture and polarity of female germline cyst in Xenopus. Developmental Biology 266, 43-61. DOI: https://doi.org/10.1016/j.ydbio.2003.10.002.

Kloc, M., Bilinski, S., & Etkin, L. D. (2004). The Balbiani Body and Germ Cell Determinants: 150 Years Later. Current Topics in Developmental Biology, 59, 1-36. DOI: https://doi.org/10.1016/S0070-2153(04)59001-4

Lawson, K. A., Dunn, N. R., Roelen, B. A. J., Zeinstra, L. M., Davis, A. M., Wright, C. V. E., Korving, J. P. W. F. M., & Hogan, B. L. M. (1999). Bmp4 is required for the generation of primordial germ cells in the mouse embryo. Genes and Development, 13(4), 424-436. https://doi.org/10.1101/GAD.13.4.424

Lei L, & Spradling AC. (2013). Female mice lack adult germ-line stem cells but sustain oogenesis using stable primordial follicles. Proc. Natl. Acad. Sci. 110, 8585-8590. DOI: https://doi.org/10.1073/PNAS.1306189110/-/DCSUPPLEMENTAL

Lei L., & Spradling, A. C. (2016). Mouse oocytes differentiate through organelle enrichment from sister cyst germ cells. Science (New York, N.Y.), 352, 95. DOI: https://doi.org/10.1126/SCIENCE.AAD2156

Levy E. W., Leite, I., Joyce, B. W., Shvartsman, S. Y., & Posfai, E. (2024). A tug-of-war between germ cell motility and intercellular bridges controls germline cyst formation in mice. Current Biology 34, 5728-5738. e4. DOI: https://doi.org/10.1016/j.cub.2024.10.062

Lieber, T., Jeedigunta, S. P., Palozzi, J. M., Lehmann, R., & Hurd, T. R. (2019). Mitochondrial fragmentation drives selective removal of deleterious mtDNA in the germline. Nature, 570, 380-384. DOI: https://doi.org/10.1038/s41586-019-1213-4

Lighthouse D, Buszczak M, & Spradling AC. (2008). New components of the Drosophila fusome suggest it plays novel roles in signaling and transport. Developmental Biology 317, 59-71. https://doi.org/10.1016/J.YDBIO.2008.02.009

Lin H, Yue L, & Spradling AC. (1994). The Drosophila fusome, a germline-specific organelle, contains membrane skeletal proteins and functions in cyst formation. Development 120, 947-956. DOI: https://doi.org/10.1242/DEV.120.4.947

Littlefield CL. (1994). Cell-cell interactions and the control of sex determination in hydra. Semin. Dev. Biol.5, 13-20. https://doi.org/10.1006/sedb.1994.1003

Liu, Y., Lau, X., Munusamy, P., Sanchez, C. M. A. S., Snell, D., & Sangrithi, M. (2025). Single-cell RNA-seq identifies protracted mouse germline X chromosome reactivation dynamics directed by a PRC2-dependent mechanism. *Developmental Cell*, *60*(9), 1321-1335.e5. https://doi.org/10.1016/J.DEVCEL.2024.12.028/ASSET/714FBA10-362A-4CC7-AA61-56D56DC3A471/MAIN.ASSETS/GR4.JPG

Loda, A., Collombet, S., & Heard, E. (2022). Gene regulation in time and space during X-chromosome inactivation. *Nature Reviews Molecular Cell Biology 2022 23:4*, *23*(4), 231-249. https://doi.org/10.1038/s41580-021-00438-7.

Lu, K., Jensen, L., Lei, L. and Yamashita, Y. M. (2017). Stay Connected: A Germ Cell Strategy. *Trends Genet.* 33, 971–978.

Machamer CE (2008). The Golgi complex in stress and death. Frontiers in neuroscience. 9, 421.

Mahowald, A. P., & Strassheim, J. M. (1970). Intercellular migration of centrioles in the germarium of Drosophila Melanogaster: An electron microscopic study. Journal of Cell Biology, 45, 306-320. DOI: https://doi.org/10.1083/JCB.45.2.306

Marlow, F. L., & Mullins, M. C. (2008). Bucky ball functions in Balbiani body assembly and animal-vegetal polarity in the oocyte and follicle cell layer in zebrafish. *Developmental Biology*, *321*(1), 40-50. https://doi.org/10.1016/j.ydbio.2008.05.557.

Matova N, Cooley L. (2001). Comparative aspects of animal oogenesis. Developmental Biology 231:291–320. DOI: https://doi.org/10.1006/dbio.2000.0120, PMID: 11237461

Meiring, J. C. M., Shneyer, B. I., & Akhmanova, A. (2020). Generation and regulation of microtubule network asymmetry to drive cell polarity. Current Opinion in Cell Biology 62, 86-95. https://doi.org/10.1016/J.CEB.2019.10.004

Mercer, M., Jang, S., Ni, C., & Buszczak, M. (2021). The Dynamic Regulation of mRNA Translation and Ribosome Biogenesis During Germ Cell Development and Reproductive Aging. Frontiers in Cell and Developmental Biology, 9. DOI: https://doi.org/10.3389/FCELL.2021.710186

Mitra, S., & Ryoo, H. D. (2019). The unfolded protein response in metazoan development. Journal of Cell Science, 132(5). https://doi.org/10.1242/JCS.217216/57527

Monteiro VL, Safavian D, Vasudevan D, Hurd TR. (2023). Mitochondrial remodelling is essential for female germ cell differentiation and survival. PLoS Genet. 19, e1010610. doi: 10.1371/journal.pgen.1010610.

Moore, C. A., & Zernicka-Goetz, M. (2005). PAR-1 and the microtubule-associated proteins CLASP2 and dynactin-p50 have specific localisation on mouse meiotic and first mitotic spindles. Reproduction, 130, 311-320. DOI: https://doi.org/10.1530/REP.1.00651

Nicholls, P. K., Schorle, H., Naqvi, S., Hu, Y. C., Fan, Y., Carmell, M. A., Dobrinski, I., Watson, A. L., Carlson, D. F., Fahrenkrug, S. C., & Page, D. C. (2019). Mammalian germ cells are determined after PGC colonization of the nascent gonad. Proc. Natl. Acad. Sci. USA, 116, 25677-25687. DOI: https://doi.org/10.1073/pnas.1910733116

Niu, W., & Spradling, A. C. (2022). Mouse oocytes develop in cysts with the help of nurse cells. Cell 185, 2576-2590. e12. https://doi.org/10.1016/J.CELL.2022.05.001

Nogawa, T., Sung, W. K., Jagiello, G. M., and Browne, W. (1988). A quantitative analysis of mitochondria during fetal mouse oogenesis. J. Morphol. 195, 225–234.

Palozzi, J. M., Jeedigunta, S. P., Minenkova, A. v., Monteiro, V. L., Thompson, Z. S., Lieber, T., & Hurd, T. R. (2022). Mitochondrial DNA quality control in the female germline requires a unique programmed mitophagy. Cell Metabolism, 34, 1809-1823.e6. https://doi.org/10.1016/j.cmet.2022.10.005

Pang, L. Y., DeLuca, S., Zhu, H., Urban, J. M., & Spradling, A. C. (2023). Chromatin and gene expression changes during female Drosophila germline stem cell development illuminate the biology of highly potent stem cells. ELife, 12. DOI: https://doi.org/10.7554/ELIFE.90509

Pepling, M. E., & Spradling, A. C. (1998). Female mouse germ cells form synchronously dividing cysts. Development 125, 3323-3328. https://doi.org/10.1242/DEV.125.17.3323

Pepling, M. E., & Spradling, A. C. (2001). Mouse ovarian germ cell cysts undergo programmed breakdown to form primordial follicles. Dev. Biol., 234(2), 339-351. https://doi.org/10.1006/DBIO.2001.0269

Pepling, M. E., Wilhelm, J. E., O'Hara, A. L., Gephardt, G. W., & Spradling, A. C. (2007). Mouse oocytes within germ cell cysts and primordial follicles contain a Balbiani body. PNAS, *104*(1), 187-192. https://doi.org/10.1073/pnas.0609923104.

Petrella LN, Smith-Leiker T, Cooley L. (2007). The ovhts polyprotein is cleaved to produce fusome and ring canal proteins required for Drosophila oogenesis. Development 134:703–712. DOI: https://doi.org/10.1242/dev.02766, .

Petronczki, M., & Knoblich, J. A. (2001). DmPAR-6 directs epithelial polarity and asymetric cell division of neuroblasts in Drosophila. Nature Cell Biol. 3, 43-49. DOI: https://doi.org/10.1038/35050550

Planelles-Herrero, V. J., Bittleston, A., Seum, C., Gaitan, M. G., & Derivery, E. (2022). Elongator stabilizes microtubules to control central spindle asymmetry and polarized trafficking of cell fate determinants. Nature Cell Biol 24, 1606-1616. DOI: https://doi.org/10.1038/s41556-022-01020-9.

Price, K. L., Tharakan, D. M. and Cooley, L. (2023). Evolutionarily conserved midbody remodeling precedes ring canal formation during gametogenesis. *Dev. Cell* 1–15.

Reik, W., & Azim Surani, M. (2015). Germline and Pluripotent Stem Cells. Cold Spring Harbor Perspectives in Biology, 7, a019422. DOI: https://doi.org/10.1101/CSHPERSPECT.A019422

Rosario R, Crichton JH, Stewart HL, Childs AJ, Adams IR, Anderson RA. (2019). Dazl determines primordial follicle formation through the translational regulation of Tex14. FASEB J. 33, 14221-14233. doi: 10.1096/fj.201901247R.

Ruby, J. R., Dyer, R. F., and Skalko, R. J. (1969). Continuities between mitochondria and endoplasmic reticulum in the mammalian ovary. Z. Zellforsch. Mikrosk. Anat. 97, 30–37.

Ruggiu, M., Speed, R., Taggart, M., McKay, S. J., Kilanowski, F.,Saunders, P., Dorin, J., and Cooke, H. J. (1997) The mouse Dazla gene encodes a cytoplasmic protein essential for gametogenesis. Nature 389, 73–77

Saitou, M., Kagiwada, S., & Kurimoto, K. (2011). Epigenetic reprogramming in mouse pre-implantation development and primordial germ cells. Development, 139(1), 15-31. https://doi.org/10.1242/DEV.050849

Seki Y, Yamaji M, Yabuta Y, Sano M, Shigeta M, Matsui Y, Saga Y, Tachibana M, Shinkai Y, Saitou M. (2007). Cellular dynamics associated with the genome-wide epigenetic reprogramming in migrating primordial germ cells in mice. Development 134:2627-2638. DOI: https://doi.org/10.1242/dev.005611

Sicari, D., Igbaria, A., & Chevet, E. (2019). Control of Protein Homeostasis in the Early Secretory Pathway: Current Status and Challenges. *Cells 2019, Vol. 8, Page 1347*, *8*(11), 1347. https://doi.org/10.3390/CELLS8111347

Sekula, M., Tworzydlo, W., & Bilinski, S. M. (2024). Balbiani body of basal insects is potentially involved in multiplication and selective elimination of mitochondria. *Scientific Reports*, *14*(1). DOI: https://doi.org/10.1038/S41598-024-58997-6

Spradling, A. C., Niu, W., Yin, Q., Pathak, M., & Maurya, B. (2022). Conservation of oocyte development in germline cysts from Drosophila to mouse. *ELife,* 11. https://doi.org/10.7554/ELIFE.83230

Spradling, A.C. (2024). The ancient origin and function of germline cysts. Results Probl Cell Differ. 71, 3-21. DOI: 10.1007/978-3-031-37936-9.

Spradling A.C., Pathak M., Davidian A., Maurya, B., Tiwari A., Yin Q., Fu Y., & Mao A., (2025). Hypothesis: Germline rejuvenation during meiosis underlies animal oogenesis. *Developmental biology*, *527*, 65–76. https://doi.org/10.1016/j.ydbio.2025.08.002

Suda, Y., Tachikawa, H., Suda, T., Kurokawa, K., Nakano, A., & Irie, K. (2024). Remodeling of the secretory pathway is coordinated with de novo membrane formation in budding yeast gametogenesis. IScience, 27(10). DOI: https://doi.org/10.1016/j.isci.2024.110855

Sunchu, B., & Cabernard, C. (2020). Principles and mechanisms of asymmetric cell division. Development (Cambridge, England) 147, dev167650. DOI: https://doi.org/10.1242/DEV.167650

Taniguchi, M., & Yoshida, H. (2017). TFE3, HSP47, and CREB3 Pathways of the Mammalian Golgi Stress Response. *Cell Structure and Function*, *42*(1), 27–36. https://doi.org/10.1247/CSF.16023

Unal E, Kinde B, Amon A. (2011). Gametogenesis eliminates age-induced cellular damage and resets life span in yeast. Science 332, 1554-1557.

Urven, L. E., Erickson, C. A., Abbott, U. K., & McCarrey, J. R. (1988). Analysis of germ line development in the chick embryo using an antimouse EC cell antibody. Development, 103, 299-304. https://doi.org/10.1242/DEV.103.2.299.

Vember SS, Brodsky JL. (2008). One step at a time: endoplasmic reticulum-associated degradation. Nature reviews. Molecular cell biology. 9, 944-957.

Watson, J. L., Krüger, L. K., Ben-Sasson, A. J., Bittleston, A., Shahbazi, M. N., Planelles-Herrero, V. J., Chambers, J. E., Manton, J. D., Baker, D., & Derivery, E. (2023). Synthetic Par polarity induces cytoskeleton asymmetry in unpolarized mammalian cells. Cell, 186, 4710-4727.e35. https://doi.org/10.1016/J.CELL.2023.08.034.

Weismann, A., 1892. Das Keimplasma, G. Fisher, p. 1882. Jena.

Wilson EB. 1925. The Cell in Development and Heredity. 3rd edition. New York: Macmillan Co.

Yamashita, Y. M. (2023). Asymmetric Stem Cell Division and Germline Immortality. *Annual Review of Genetics*, *57*, 181-199. https://doi.org/10.1146/ANNUREV-GENET-022123-040039.

Yang, CR., Rajkovic, G., Daldello, E.M. *et al.*(2020). The RNA-binding protein DAZL functions as repressor and activator of mRNA translation during oocyte maturation. *Nat Commun* **11**, 1399. https://doi.org/10.1038/s41467-020-15209-9

Yin, Q., & Spradling, A. C. (2025). Distinct waves of ovarian follicles contribute to mouse oocyte production. BioRxiv, 2024.05.30.596686. DOI: https://doi.org/10.1101/2024.05.30.596686

Yoshinaga, K., Fujimoto, T., Nakamura, M., & Terakura, H. (1992). Selective lectin-binding sites of primordial germ cells in chick and quail embryos. The Anatomical Record 233, 625-632. https://doi.org/10.1002/AR.1092330416

Yoshinaga, K., Muramatsu, H., & Muramatsu, T. (1991). Immunohistochemical localization of the carbohydrate antigen 4C9 in the mouse embryo: a reliable marker of mouse primordial germ cells. Differentiation, 48, 75-82. https://doi.org/10.1111/j.1432-0436.1991.tb00245.x

Xiao T, Ünal E. (2025). Remodeling, compartmentalization, and degradation: a trifecta for organelle quality control during gametogenesis. Curr Opin Genet Dev. 92, 102347. doi: 10.1016/j.gde.2025.102347.

Zaffagnini G, Cheng S, Salzer MC, Pernaute B, Duran JM, Irimia M, Schuh M, Böke E. (2024). Mouse oocytes sequester aggregated proteins in degradative super-organelles. Cell 2024, 187:1109-1126 e21.

Zagore, L. L., Sweet, T. J., Hannigan, M. M., Weyn-Vanhentenryck, S. M., Jobava, R., Hatzoglou, M., Zhang, C., & Licatalosi, D. D. (2018). DAZL Regulates Germ Cell Survival through a Network of PolyA-Proximal mRNA Interactions. Cell Reports 25, 1225-1240.e6. DOI: https://doi.org/10.1016/j.celrep.2018.10.012

STAR* METHODS

Key Resource table

Reagent or Resource	Source	Identifier
Antibody/Lectin/Stains		
EMA	DSHB	EMA-1 AB_531885
GCNA	Abcam	ab82527
DDX4	Abcam/R&D systems	ab13840 & ab27591/ AF2030
SSEA1	DSHB	MC-480
WGA	Thermo Fisher	W7024
Gm-130	ThermoFisher/Novus Biologicals	610822/NBP2-53420
Rab9	Thermo Fisher	MA5-31997
Rab11a1	Thermo Fisher	700184
Tex14	Proteintech	18351-AP
GFP/YFP	Aves Labs	GFP-1020
Dazl	BioRad Labs/GeneTex	MCA2336/GTX89448
Lysotracker deep	Thermo Fisher	L7528
Pard3	Novus Biologicals	NBP1-88861
LAMP1	Cell Signaling Technology	9091T
Xbp1	Abcam	ab37152
Gs28	BD biosciences	61184
AAL	Vector Labs Inc	FL-1391-1
LCA	Vector Labs Inc	FL-1041-5
Sec63	Thermo Fisher	PA5-100180
Calnexin	Abcam	ab219644
Gs28	Proteintech	16106-1-AP
Acetyl-α-Tubulin (Lys40)	Cell Signaling. Tech	5335S
Alpha Tubulin (acetyl K40)	Abcam	ab289875
Pericentrin	Abcam	ab4448/ab28144
Anti-GCNA1 antibody	Abcam	ab82527
Rac GAP1 Antibody (A-6)	Santa Cruz Biotechnology, Inc	sc-271110
Dnmt3a	Cell Signaling. Tech	3598T
ATP5A	Abcam	ab14748
Mitotracker /Deep	Thermo Fischer	M7514/ M22426
ER-Tracker™ /	Thermo Fischer	E34251/ E34250
Quinacrine dihydrochloride	Sigma chemical	Q3251
Chemicals		

Paraformaldehyde	Electron Microscopy Sci.	15714
Tamoxifen	Sigma Chemical	T5648
Corn Oil	Sigma Chemical	C8267
Tween 20	Sigma Chemical	P1379
Triton X	Sigma Chemical	X100
Mounting media	Vector Labs Inc.	H-1000
Trypsin-EDTA (0.25%)	Fisher	25200056
Fetal Bovine serum	Sigma Chemical	F2442
Bovine serum albumin	Sigma Chemical	A4503
SSEA1 (CD15) microbeads	Miltenyi Biotech	130-094-530
DMEM/F-12	Fischer	11320-033
Celiobrevin D	Millipore	250401
Critical Commercial kits		
Kappa fast hot start ready-mix	KAPPA Biosystems	KK5608
KAPPA express extract	KAPPA Biosystems	KR0383-v4.16
10X Genomics kit		
IRE1-Xbp1 Assay	Montana Molecular	U0921G
Proteasome Activity	Amplite	13456
Superscript IV cells direct cDNA synthesis kit	Fischer	11750510
Experimental models		
C57BL/6J	Jackson Laboratory	000664
CAG-Cre-ER	Jackson Laboratory	004682
R26R-EYFP	Jackson Laboratory	006148
Dazl1L $^{-/+}$	Jackson Laboratory	035880
Others		
MACS MS separation columns	Miltenyi Biotech	130-042-201
Cell culture inserts	Millipore	PICM01250
Cell strainer	Sigma	CLS431752
Software and Algorithms		
FIJI	FIJI	Version: 2.16.0/1.54p
IMARIS	Oxford Instruments (formerly Bitplane)	Version: 10.2
SEURAT	Satija Lab	Version: 5.1.0
CELL RANGER PIPELINE	10X genomics	Version: 6.0.1/8.0.1
GRAPHPAD PRISM	GraphPad Software	Version: 10.5.0

PRIMER DETAILS

Primer Name	Sequence	Amplicon Size and Reference
Uba1_Forward	5´-TGGTCTGGACCCAAACGCTGTCCACA-3´	Male- 198 bp Female- 217 bp *McFarlane et al., 2013 (https://doi.org/10.1159/000348677)*
Uba1_Reverse	5´-GGCAGCAGCCATCACATAATCCAGATG-3´,	
Sly_Forward	5'-GATGATTTGAGTGGAAATGTGAGGTA-3'	Male- 280 bp Female- 685 and 480 bp *McFarlane et al., 2013 (https://doi.org/10.1159/000348677)*
Sly_Reverse	5'-CTTATGTTTATAGGCATGCACCATGTA-3'	
Zfy_Forward	5'-GACTAGACATGTCTTAACATCTGTCC-3'	Male- 180 bp *McFarlane et al., 2013 (https://doi.org/10.1159/000348677)*
Zfy_Reverse	5'-CCTATTGCATGGACTGCAGCTTATG-3'	
DDX4 Forward	5'-GAGATTGCCTTCAGTACCTATGTG-3'	105 bp *Gao et al., 2011 (https://doi.org/10.1095/biolreprod.110.084590)*
DDX4 Reverse	5'-GTGCTTGCCCTGGTAATTCT-3'	
GAPDH Forward	5'-GGTGAAGCAGGCATCTGAGGG-3'	246 bp *Chunmei et al., 2011 (https://doi.org/10.1093/glycob/cwq152)*
GAPDH Reverse	5'-GGTGGGTGGTCCAGGGTT-3'	
Dazl Common	5'-GAC ATT ACT AAG AAA ACA GCA GTG G-3'	Mutant=~300 bp, Heterozygote=~300 bp and 192 bp, Wild type=192 bp *JAX Protocol (Strain #035880, Primer# 56340, 56341 and 56342)*
Dazl WT reverse	5'-TTC TGC ACA TCC ACG TCA TT-3'	
Dazl Mut Reverse	5'-ATC CCT CCC TTT AGG GCT CA-3'	

RESOURCE AVAILABILITY

Lead contact Further information and requests for resources and reagents should be directed to and will be fulfilled by the Lead Contact, Allan C. Spradling (spradling@carnegiescience.edu).

Materials availability

This study did not generate new unique reagents.

Data availability

Raw sequencing data has been deposited at Gene Expression Omnibus (GEO)

database (accession: GSE303512). Any additional information required to reanalyze

the data reported in this paper is available upon request.

EXPERIMENTAL MODEL AND SUBJECT DETAILS

Mouse strains used-C57BL/6, CAG-cre/ERT2 mice, R26R-EYFP (as described in Lei and Spradling, 2016) and Dazl1L$^{+/-}$ mice (Strain #035880 from JACKSON laboratories). Genotyping was performed according to protocols provided by the JAX Genotyping was performed according to protocols from the JAX Mice database. Animals were provided with a proper light-dark cycle, temperature, humidity, food and water. Sexually mature females and males (6-8 weeks old) were kept for mating. Mating was confirmed through the observation of a vaginal plug. As per standard protocol, we designate the midday of the corresponding day as E0.5, which marks the beginning of embryonic development. Fetal gonads were dissected during E10.5-E18.5 as needed. The day pups are born is designated as P0 and were dissected for some experiments. The Institutional Animal care and use committee of Carnegie Institution of Washington approved procedures for animal handling and experimentation.

METHOD DETAILS

Single germ cell lineage labeling

The protocol used for single germ cell lineage labeling was performed as described previously (Lei and Spradling, 2016). Briefly, to obtain fetuses for lineage marking, adult female R26R-EYFP mice were mated with male CAG-cre/ERT2 mice. Tamoxifen was dissolved in corn oil (Sigma) and a single dose was injected intraperitoneally at 0.2 mg per 40 g body weight into pregnant female R26R-EYFP mice at E10.5. Fetal gonads/Pups were dissected as needed in between E11.5-E18.5/P0. To analyze the lineage-labeled germ cells, fixed and frozen whole gonads were subjected to whole mount staining for chicken-GFP, the number of lineage-labeled

germ cells of each ovary was determined by examining optically sectioned Z-stack images generated by confocal imaging of the entire ovary.

Immunostaining

Dissected fetal gonads/ovaries were washed in Phosphate buffer saline (PBS) and fixed immediately in cold 4% paraformaldehyde overnight at 4^0 C. Following the fixation, the gonads were washed three times with $PBST_2$, which is a mixture of phosphate-buffe saline (PBS) with 0.1 % Tween 20 (Sigma) and 0.5 % Triton X (Sigma). Each wash cycle lasted for 30 minutes. Next, gonads were Incubated with primary antibodies mixed with Blocking solution ($PBST_2$+ 10 % Normal donkey serum) overnight at room temperature. Following day, gonads were incubated with fluorescein-conjugated secondary antibodies (Donkey Anti-Rabbit/mouse/rat Alexa-fluor 488/568/647, Invitrogen) overnight at room temperature. Next day, gonads were washed with PBST and stained with DAPI (Sigma) to visualize nuclei. Gonads were mounted on slides with a mounting medium (Vector Labs) and analyzed using confocal microscopy (STELLARIS 8 DIVE Multiphoton Microscope, Leica). Germ cell numbers are quantified in each ovary by manually counting EMA/DDX4 stained germ cells in multiple 0.45 µm optical sections from different ovaries.

3D reconstruction

Three-dimensional model images and movies were generated by Imaris software (Bitplane).For z-stack images, different visualization options in the Surpass mode of Imaris helped to gain visualization control of the objects. To perform surface rendering and volume quantification using Imaris software, we imported your 3D image dataset for EMA/WGA staining. We started with a “Volume” rendering for channels corresponding to EMA/WGA staining and then we adjusted the contrast, brightness and transparency in the “Display

Adjustment" window. Next, we used the Surfaces module to create surface renderings by selecting the appropriate fluorescence channel, applied manual thresholding and adjusted smoothing parameters to define the structure accurately. Once the surface is rende, we navigated to the statistics tab to access volume measurements. Further visualization of the results was performed in 3D or orthogonal views to confirm accuracy, and adjusted rendering properties such as color or transparency as needed. To create spots for easy counting of labelled cells, we used the "Spots" icon-option in the "Creation" menu and started the spot creation wizard. We set the approximate spot size as per the requirement. Next, we selected the "Manual Creation" option to place spots individually. Each click placed a single spot at the corresponding position.

Sexing and Genotyping

Tail samples from mouse were collected and subjected to lysis and DNA extraction using Proteinase K based lysis buffer treatment at 55^0C overnight followed by 95^0C incubation for 10 minutes. The samples were then centrifuged at 14000 rpm for 5 min to pellet the debris. Extracted genomic DNA from supernatant was used directly and amplified with the Uba1, Sly and Zfy primer pairs for sex determination (McFarlane et al., 2013, Table S2). PCR reactions were performed using KAPA Fast Hotstart ReadyMix with dye (Kappa Biosystems, #KK5608) using the following PCR parameters: initial denaturation at 95 ° C for 5 min, 35 cycles with 94 °C for 30 s, 60° C and 72° C for 30 s, followed by final elongation at 72° C for 5 min. PCR products were analyzed with a DNA ladder (100 bp) on 2% agarose gels and visualized with ethidium bromide under UV-illumination. The male and female amplicon can be distinctly visualized due to different amplicon sizes of PCR products (See Primer details).

Electron microscopy

Whole ovaries were dissected in PBS and fixed in 4% Paraformaldehyde overnight. After three 3-min washes in cacodylate buffer, ovaries were postfixed in 1% OsO4, 0.5% K3Fe {CN)6, in cacodylate buffer for 1 hour and were rinsed twice for 5 min in cacodylate buffer and once for 5 min with 0.05 M maleate (pH 6.0). The ovaries were stained in 0.5% uranyl acetate overnight at 4 degrees rinsed in water and dehydrated through an ethanol series. Following two 10-rain washes with propylene oxide, the ovaries were infiltrated with resin. The resin-embedded specimen was polymerized by incubation at 45^0 C and 70^0 C for 12 hours each. Silver-gold sections were cut, stained with lead citrate, and observed in the electron microscope.

Single cell RNA sequencing of Wildtype E10.5, E11.5 and E15.5 gonad

Embryonic ovaries were dissected such that individual fetal gonad at E10.5 (18 gonads from 3 females), E11.5 (12 female gonad from 3 females) and E15.5 (10 gonad from 2 females) were collected. For E10.5 and E11.5: corresponding tail were labelled for identification and placed in 1× PBS on ice. We performed quick Quinacrine and DAPI staining (~15 min) of corresponding E10.5 and E11.5 fetal tail samples to eliminate the male gonad samples -with positive Quinacrine staining of tail samples. We then pooled the dissected female gonad sample and dissociated it into single cells using 0.25% Trypsin at 37^0 C for 5-7 min with two pipet trituration in between. Fetal bovine serum (10 %) was then used to neutralize trypsin. Dissociated cells were passed through 100-µm strainer. The cell suspension was centrifuged at 300 g for 5 minutes and cell pellet was resuspended in freshly prepared and filter-sterilized 0.04% BSA. Viability of cells was assessed via trypan staining and >90 percent viable samples were selected and loaded (~10000 live cells for E11.5 and E15.5, ~20000 cells for E10.5) onto the 10X Genomics Chromium Single Cell system using the for E11.5 and E15.5-v3 and for E10.5 v4 chemistry as per the manufacturer's instruction. Single-cell RNA capture and library

preparations were performed, and standard data was data processing was performed using Cell ranger pipeline (6.0.1 - for E11.5 and E15.5 and 8.0.1-for E10.5) and later data was visualized and analyzed by Seurat v5.1.0.

Single cell RNA sequencing of Dazl1L mutant gonad

Dazl+/- female and males were kept for mating and plugged females were marked as E0.5. The gonad from E11.5, E12.5 fetuses were dissected, fetuses were collected in and kept in cold PBS in 12-well plate such that each well with individual fetus is marked for identification. Fetal tails were collected, labelled and subjected to kapa express extract kit (Catalog #KR0383-v4.16) mediated fast DNA extraction according to manufacturer's protocol. Briefly, one step lysis and DNA extraction system was set up in 100 µl volume by adding 10 µl express extract buffer, 2 µl of express extract enzyme and 88 µl of PCR grade water in each tail sample followed by 75^0 C incubation in heating block for 15 minutes for lysis. The samples were then incubated at 95^0C in heating block for 5 minutes for DNA extraction. The sample was then centrifuged briefly to pellet the debris, and supernatant was used directly for PCR as mentioned in methods section of RNA isolation, cDNA synthesis and PCR. The standard genotyping JAX protocol for strain 035880 is refer to identify homozygous / heterozygous and wild type fetuses. Simultanoeusly male/female sexing was also performed (primer details in Table S2). After correct identification, homozygous fetuses-from E11.5 (6 gonad from 3 females) and E12.5 (6 gonad from two females)- were trypsinized to prepare live single cells which were then subjected to 10X Genomics Chromium (v3 chemistry) and data was processed using cell ranger pipeline 6.0.1 and analyzed using seurat v5.1.0 in same manner as mentioned previously for E11.5 gonad.

Cell Identification and Clustering Analysis

Single-cell RNA sequencing (scRNA-seq) data were analyzed using the Seurat package (v5.1.0, https://satijalab.org). Count data generated by the Cell Ranger pipeline (6.0.1/8.0.1) were imported into R using the Read10X function and converted into a Seurat object with the CreateSeuratObject function. R packages were used to filter out the low-quality cells, and the following criteria were used to filter cells:

a) **for E10.5 WT gonad**: nFeature_RNA > 500 & nFeature_RNA<8500 & nCount_RNA > 500 & percent.mt<5

b) **for E11.5 WT gonad**: nFeature_RNA > 100 & nFeature_RNA<11000 & nCount_RNA > 300 & percent.mt<10

c) for E15.5 WT ovary: nFeature_RNA > 500 & nFeature_RNA<9000 & nCount_RNA > 500 & percent.mt<10.

The filte count matrices were Log-normalized using the "NormalizeData" function and scaled with the "ScaleData" function to prepare for dimensionality uction. "Principal Component Analysis (PCA)" was then applied to uce dimensionality, followed by using top 15 dimensions and default resolution to cluster cells based on gene expression profiles using the "FindNeighbors" and "FindClusters" functions. Cell populations were visualized using the umap method, facilitating the identification of distinct cell types.

Bioinformatic segregation of female germ cells

To segregate E10.5 and E11.5 XX-specific germ cells with complete surety we performed bioinformatic segregation of female germ cells to address the limitations of primitive Quinacrine staining. The expression of the X-linked gene Xist, Ddx3x, Utx etc., were used as a marker. Cells with significant Xist or other X-linked gene expression expression were labeled as "XXonly" using the "Idents" and "WhichCells" R functions. A new Seurat object containing only XX-specific cells was created using the subset function. Germ cells within this subset were identified by examining the expression of germ cell-specific marker genes, and a further subset of E10.5

and E11.5 female germ cells was created using the subset function to focus on germ cells specifically.

Wildtype ger cells-merged dataset creation and Validation

ScRNA-seq datasets from E11.5 to P5 (retrieved from the GEO database, GSE136441 and merged object submiited to Github) were visualized using Seurat. E11.5 cells were discarded and new merged dataset from E10.5-P5 was created, subsets of germ cell clusters from E10.5, E11.5, and E15.5 were integrated using Seurat's “Merge” function. The resulting merged dataset was then processed by normalizing and scaling the data, followed by the identification of variable genes. Th ebatch correction was performed using and pre-harmony and post-harmony data was assessed by visualizing LISI (Local Inverse Simpson’s Inde) score confirming successful batch mixing. Cell clusters were determined using Seurat's sha nearest neighbor (SNN) algorithm with PCA uction using top 15 dimesnions and 2.8 resolution. To visualize these clusters, dimensionality uction was applied (umap) with following criteria: RunUMAP(new_merge, dims=1:15, n.neighbors=40, min.dist=0.6, spread=1) enabling the identification of distinct cell populations.

Cell cycle stages of germ cells across the different developmental stages (E10.5-P5) were validated by visualizing meiosis stage specific expression pattern via feature plot. This visualization technique allows for the capture of subtle trends and helps in comparing expression peaks, providing insights into the transition from mitosis to meiosis across the different developmental stages. Additionally, a violin plot was employed to visualize the variability in average raw UMI levels across germ cells. This approach allowed for an effective comparison of gene expression profiles, highlighting the differences in gene expression patterns between different stages.

Dazl mutant merged dataset

For E11.5 and E12.5 Dazl$^{-/-}$ dataset, cells were filte based on following criteria:

a) **for E11.5 Dazl -/- ovary** : nFeature_RNA > 500 & nFeature_RNA<9000 & nCount_RNA > 500 & percent.mt<5

b) **for E12.5 Dazl-/- ovary** nFeature_RNA > 500 & nFeature_RNA<10000 & nCount_RNA > 500 & percent.mt<5

Top 15 dimensions were used at default resolution to cluster the cells which were then visualized by umap. To create merged dataset from subset containing only germ cells were created and merged using "merge" function as described previously. Three dataset were created -for E11.5 wildtype and Dazl$^{-/-}$ dataset, for E12.5 and Dazl-/- dataset and one dataset was created where both E11.5 and 12.5 WT and Dazl-/- were merged. Batch correction was applied using harmony. Merged dataset was normalized, scaled and top 15 dimensions at resolution of 0.4 was used for visualization using umap.

***In vitro* gonad culture: microtubule inhibitor/BFA treatment and organelle tracker assay**

To perform in vitro culture of mouse fetal ovaries on membrane inserts with or without inhibitors, we prepared sterile culture medium, constituting DMEM/F-12 supplemented with 10% fetal bovine serum and penicillin-streptomycin. Inhibitor stock solutions were prepared in DMSO and diluted at desi concentration in culture media (Ciliobrevin D from Millipore, 25 μM for 6 hours, BFA from Invitrogen, 5μg/ml for 6 hours). Control medium containing the vehicle DMSO was prepared simultaneously. Fetal ovaries were dissected from E11.5 embryos under a stereomicroscope in sterile PBS, we have kept the surrounding mesonephric tissue intact and attached to the gonad to ensure proper development. We have also collected corresponding fetus tail of each fetal gonad to perform genetic sex determination. We have placed membrane inserts into a 24-well plate and added ~500 μL of culture medium (with or without inhibitors) to the

lower chamber and ensu no contact between medium and the insert surface. Next, we gently placed isolated ovaries onto the membrane surface using sterile forceps. The plate is then incubated in a CO_2 incubator at 37°C for ~6 hours. After the designated culture period, confirmed ovaries (post genetic-sex analysis), were carefully removed from the membrane inserts and washed three times with basal media to remove any residual inhibitors. Next, we collected ovaries and fixed in 4% PFA for downstream immunolocalization studies. To inhibit the microtubule growth using cold treatment, we transfer dissected gonad to a chilled culture medium, maintained at 0-4°C. The tissue is fully immersed in the pre-cooled medium and incubated on ice for ~60 minutes. This low-temperature exposure destabilizes microtubules by disrupting tubulin dynamics, effectively depolymerizing existing microtubules and inhibiting further polymerization. After the incubation, the tissue is washed with fresh ice-cold medium and fixed in 4% PFA. To stain specifically for organelles: Fetal ovaries were dissected and cultu in vitro in DMEM/F12 medium supplemented with organelle-specific fluorescent dyes. LysoTracker™ Deep (Thermo Fisher, L7528, 1 mM stock) or MitoTracker™ (Thermo Fisher, M7514) or MitoTracker™ Deep (Thermo Fisher, M22426), and ER-Tracker™ (Thermo Fisher, E34251) or ER-Tracker™ (Thermo Fisher, E34250) were each added at a final concentration according to the manufacturer's recommendations. The ovaries were incubated in this dye-containing medium at 37 °C with 5% CO_2 for 12 hours. Following incubation, tissues were collected and fixed in 4% paraformaldehyde (PFA) for subsequent immunostaining.

Magnetic activated cell sorting (MACS)

Embryonic ovaries were pooled and treated with Trypsin then were neutralized followed by centrifugation as mentioned before to in scRNA Sequencing method section to create dissociated single cells. The resulting cell pellet was re-suspended in ~80 microliters MACS

buffer i.e. PBS with 0.5% BSA and 2 mM ethylene diaminetetraacetic acid (EDTA). ~20 microliters Anti-SSEA1 (CD15) microbeads (MiltenyiBiotec Inc., #130-094-530) were added to the cell suspension followed by incubated for 20 min on ice. After adding 1 ml MACS Buffer to the suspension, the SSEA1 bound cells were pelleted by centrifugation at 300 g for 10 min at 4ºC. SSEA1+ve and SSEA1-ve cells were then separated by applying cell suspension to MS columns according to the manufacturer's instruction (MiltenyiBiotec Inc.). The SSEA1+ve cells were retained by the column and were filte thrice to obtain pure germ cell population. The cells were counted, and viability was assessed via trypan staining and using automated cell counter (Fischer Scientific). For validation of MACS protocol the cells were fixed in 4 % PFA to perform Immunostaining of DDX4 and were also sto in trizol to perform RNA synthesis and PCR for germ cell specific gene expression.

IRE1-Xbp1 Assay

The IRE1-XBP1 ratiometric assay (from Montana Molecular #U0921G) is a genetically encoded biosensor system utilizes a BacMam Vector carrying dual-fluorescence biosensor. For each assay reaction 50 µl transduction mix consisting of XBP1-IRE1 sensor (15 µl) plus sodium butyrate (0.6 µl per well) was prepared in basal media. To standardize the working conditions, manufacturer provided thapsigargin (1 µm per well) was used as positive control and untransduced cells were used as negative control. For each experiment equal amounts of SSEA1-ve and SSEA1 +ve cells were added to a 96-well plate in duplicates. ~50 microliters of transduction mix was added to each reaction well. The plate was incubated for 45 minutes at room temperature and then transfer to 5% CO2 and 37ºC for 24 hrs. The enzymatic activity was then measured at 37ºC by monitoring XBP1-IRE-1 sensor's fluorescent intensity (top read) at Ex/Em=488/525 nm and basal constitutive fluorescent intensity at 565/620 using microplate

reader (BioTek Synergy H1). IRE1-Xbp1 assay comparing MACS sorted SSEA1^{+} germ vs SSEA1^{-} somatic cells at E11.5 was performed across 6 experiments (~32 mice, ≥5 mice and >=20 ovaries per experiment). IRE1-Xbp1 assay comparing SSEA1^{+} vs SSEA1^{-} E12.5 cells in WT or Dazl mutant mouse across 3 experiments (~40 mice, ≥5 mice and >=25 ovaries per experiments)

20S Proteasome activity assay

To perform proteasome activity assay (Amplite #13456) we followed manufacturer's instructions. We first standardized the working conditions using trypsin enzyme as technical positive control. Trypsin is loaded on different well in different concentrations in duplicates. Blank medium along with assay buffer were added in separate wells to act as Negative control. For each experiment equal amounts of SSEA1-ve and SSEA1 +ve cells were added to a 96-well plate in duplicates. ~50 microliters of working solution consisting of fluorogenic substrate in assay buffer (prepared according to manufacturer's instructions) were added and plate was incubated for 2 hours at 37°C. The enzymatic activity was then measured at 37°C by monitoring fluorescent intensity (top read) at Ex/Em=490/525 nm (Cut off =515 nm) using microplate reader (BioTek Synergy H1). Proteasome activity in MACS-sorted SSEA1^{+} vs SSEA1^{-} cells were assessed using 3 biological assays with ~35–60 E11.5 ovary per assay. Proteasome activity ratio of MACS-sorted SSEA1^{+} and SSEA1^{-} cells compared at E12.5 with ~25–28 E12.5 ovaries were used per assay.

RNA isolation and cDNA synthesis

Total RNA was extracted using TRIzol reagent (Invitrogen) following the manufacturer's instructions. Briefly, tissue samples were homogenized in TRIzol, or cells were incubated in

TRIzol for 5 min at RT, followed by phase separation with chloroform (200 µl/ml TRIzol, shake for 10-15 seconds and keep at RT for 5 min) and centrifugation at 12,000 × g for 15 minutes at 4°C. The aqueous phase was collected, and RNA was precipitated with equal amount of isopropanol (10 min RT then same centrifugation as last step), washed with 75% ethanol, centrifuged, removed the supernatant ethanol and air-dried. Resuspended pellet in RNase-free water. RNA quality and concentration were determined spectrophotometrically. For cDNA synthesis we used Superscript IV cells Direct cDNA synthesis kit (Invitrogen, #11750150) with and modified manufacturer's protocol. We skipped the lysis step and directly added DNASe I to our sample (0.5 µl each) followed by 10 minutes incubation on ice. Then we added Stop solution (3 µl each) and kept the mixture at RT for 2 minutes. Then we set up RT reaction as per manufacturer's instruction by adding 8 µl of RT mix to each sample and setting up the following reaction in PCR thermocycler: 25^0 C for 10 min, 55^0 C for 10 min, 85 ^{0} C for 5 min and hold at 4 ^{0} C. cDNA was used directly for PCR as mentioned in Sexing and genotyping using DDX4 and GAPDH Primers (See Primer details)**.**

QUANTIFICATION AND STATISTICAL ANALYSIS

Quantification of germ cell numbers

PFA fixed ovaries were subjected to whole mount immunostaining as described previously. Z-stack images for whole ovaries were analyzed using FIJI. Germ cell numbers are quantified in each ovary by manually counting EMA/DDX4 stained germ cells in multiple 0.45 µm optical sections from different ovaries using FIJI.

3D volume Quantification

Whole mount immunostaining was performed and the z-stack images were converted to 3D image to analyze using Imaris as described previosuly. After using the Surfaces module to create surface rendering and applying manual thresholding and smoothing to define the structure accurately, we navigated to the statistics tab to access volume measurements. Further visualization of the results was performed in 3D or orthogonal views to confirm accuracy, and adjusted rendering properties such as color or transparency as needed. On an average the average values from three measurements performed were conside and plotted as graph using Graphpad prism.

Area of staining quantified using FIJI

Images were analyzed using FIJI to calculate area of staining by selecting region of interest and using measure command from Analyze tab. The results were plotted as number of pixels to depict the area corresponding to stained regions.

Statistics

Data are presented as mean ± SEM (standard error of the mean). Statistical analyses were performed using Student's paired t-test, one-way ANOVA with Tukey's post-hoc test, or the Friedman test with Dunn's post-hoc test for non-parametric data. Significance is indicated as follows: $p < 0.05$ (*), $p < 0.01$ (**), $p < 0.005$ (***), and $p < 0.001$ (****). Each experiment was performed on "N" individual specimens, as indicated in the figure legend, from at least three different animals.

SUPPLEMENTARY REFERENCES

McFarlane, L., Truong, V., Palmer, J. S., & Wilhelm, D. (2013). Novel PCR Assay for Determining the Genetic Sex of Mice. *Sexual Development*, *7*(4), 207-211. https://doi.org/10.1159/000348677

Gao, L., Kim, Y., Kim, B., Lofgren, S. M., Schultz-Norton, J. R., Nardulli, A. M., Heckert, L. L., & Jorgensen, J. S. (2011). Two Regions Within the Proximal Steroidogenic Factor 1 Promoter Drive Somatic Cell-Specific Activity in Developing Gonads of the Female Mouse. *Biology of Reproduction*, *84*(3), 422-434. https://doi.org/10.1095/BIOLREPROD.110.084590

Chunmei, W., Huang, C., Gu, Y., Zhou, Y., Zhu, Z., & Zhang, Y. (2011). Biosynthesis and distribution of Lewis X- and Lewis Y-containing glycoproteins in the murine male reproductive system. *Glycobiology*, *21*(2), 225-234. https://doi.org/10.1093/GLYCOB/CWQ152

Supplementary Video Link and legends:
Here is the link to Videos use in supplementary figures:
https://drive.google.com/drive/folders/1XuOoesa_WKMJUaVTpOKGbWWhn_fJc56M

Supplementary Video legends

Video S1A: E13.5 ovary stained GCNA in Green and EMA in Red

Video S1B: E12.5 ovary stained with YFP in Green, EMA in Red, DAPI in Blue

Video S1D1: E13.5 ovary stained for GCNA in Green, DAPI in Blue and EMA in Red

Video S1D2: E13.5 ovary, same region as S3D1 stained for GCNA in Green, and EMA in Red

Video S1I1. Successful Golgi formation within germ cells of in-vitro cultured fetal gonads.
Untreated E11.5 gonads cultured for 6 hours show intact Golgi structures within DDX4^{+} germ cells. DDX4 (red), Golgi (green), and DAPI (blue).

Video S1I2. Validation of Brefeldin A (BFA) effect on Golgi formation.
E11.5 gonads cultured for 6 hours in the presence of BFA display a complete loss of detectable Golgi structures, confirming the efficacy of BFA treatment. DDX4 (red), Golgi (green), and DAPI (blue).

Video S1I3. Reversibility of BFA treatment.
Following 6 hours of BFA exposure, withdrawal of the drug results in the successful restoration of Golgi structures-post 24 hours-in E11.5 gonads, demonstrating reversible inhibition. DDX4 (red), Golgi (green), and DAPI (blue).

Video S2A1-S2A5: E11.5 gonadal tissue stained for EMA in Red, Ac. Tub. In Green and DAPI in Blue

Video S2F: 3D modelling of fusome in E12.5 lineage labelled 8-cell cyst: YFP in Green, EMA in White and Ac. Tub in Red. Green spheres are spots generated using Imaris software to count lineage labelled cells and Grey surface rendering was performed to visualize the EMA volume.

Video S3A: E13.5 Ovary stained for PARD3 in Red, EMA in Green and DAPI in Blue.

Video S3B1: E13.5 Ovary stained for GCNA in Blue, PARD3 in Red and EMA in Green

Video S3B2: E13.5 Testis stained for GCNA in Blue, PARD3 in Red and EMA in Green

Video S5C: 3D surface rendering of E17.5 ovary: WGA in Red enriched within region spanning ring canal stained by Tex14 in Yellow and GCNA stained germ cells are shown in Green.

Video S5D: E18.5 Ovary stained of WGA in Red, GCNA in Green and DAPI in Blue

Video S5 E1-E3: E18.5 Wildtype (E1), E18.5 Dazl +/- (E2) and E18.5 Dazl -/- (E3) stained for GCNA in Green and WGA in Red

Video S5 F1-F3: P0 Wildtype (F1), Dazl +/- (F2) and Dazl -/- (F3) stained for GCNA in Green and PARD3 in Red

SUPPLEMENTARY FIGURE LEGENDS

Fig. S1: **EMA/Lectin-stained aggregate (Mouse fusome) distribution in pre-meiotic PGCs** (A) Immunostaining of E9.5-E12.5 ovary for germ cell specific marker EMA (Red) and DAPI (Blue) and for E13.5 ovary (EMA in Red, GCNA in green, Z-stack video see Video S1A). (B) Z-stack video of E12.5 ovary stained for EMA (Red), DAPI (Blue) and lineage labelling shown via YFP (Green) (See Video S1B). (C) Volume rendering of EMA aggregate (White arrows) within lineage labelled cyst (Green, YFP) using Imaris software. (D-D') Videos of at E13.5 ovary stained for EMA (Red), GCNA (Green) and DAPI (Blue) (see Video S1D1 and S1D2). (E) Random 3-D sampling using Imaris for E13.5 ovary showing branched mouse fusome structure within GCNA labelled female germ cells. (E') Representative image depicting sampling of E13.5 male gonad stained for EMA (Red), DAPI (Blue) and GCNA (Green). (F) Images of different E13.5 ovary stained for EMA (Red), GCNA (Green), Tex14 (Yellow) and DAPI (Blue). Central region with enriched fusome is often associated with higher number of ring canals. (G) E11.5 ovary stained for WGA (Red) and YFP (Green) as lineage labelling marker. Dotted line marks the WGA aggregate within germ cells. (G') E13.5 ovary stained for WGA (Red), GCNA (Green) and Tex14 (yellow) forming branched WGA-stained Mouse Fusome structure (dotted lines). (H) Co-localization of Golgi and fusome. E11.5 gonad stained for Golgi markers Gm-130 (Green) and Gs28 (Green) along with EMA (Red) and DAPI (Blue). (I) Brefieldin A (BFA; Golgi inhibitor) treatment of gonad in-vitro and recovery without Brefieldin A is shown. Z-stack videos of Untreated/BFA treated/Recovered E11.5 gonad stained for DDX4 (Red), Golgi (Green) and DAPI (Blue). I-I' Images for Untreated/BFA treated/Recovered E11.5 gonad stained for DDX4

(Red), Golgi (Green) and DAPI (Blue) validating successful reversible inhibition of Golgi formation by BFA I" is gonad stained for EMA (Red), Golgi (green) and DAPI (Blue) depicting Golgi-dependent formation of fusome. **(**J and J') E11.5 gonad stained for general fucosylation specific lectins, AAL/LCA (Green), DAPI (Blue) and fusome marker EMA (Red). (K and K') Localization of ER markers in vicinity to fusome is validated by staining ER-specific Sec63 or Calnexin (Green), DAPI (Blue) and EMA (Red). (L) Electron microscopy of E11.5 gonad depicting Golgi clusters (Dotted red lines, labelled as Fusome) near intercellular bridges (IB marked by red solid arrows). Scale bar. 100 µm (A), 20 µm (B), 10 µm (in D-K).

Fig. S2. **Validating microtubule dependent fusome formation and its distribution during cyst fragmentation.** (A) Z-stack videos for images used in figure 3A (See Videos from S2A1 to S2A5). (B) E11.5-E12.5 ovary stained for EMA (Red), Pericentrin (PCNT, Green), Ac. Tub (Grey) and DAPI (Blue). Arrows mark duplicated centrosome during Interphase. Dotted circles mark centrosomes. Smooth line marks the DAPI stained region during Anaphase depicting clear separation of Nuclei. (C) E10.5 gonad stained for EMA (Red) and Ac. Tub. (Green) Dotted line marks the newly formed fusome as spindle remnant. (D) Fusome asymmetry arises during cytokinesis depicted in E11.5 ovary stained for EMA (Red). (E) E10.5 PGCs stained for Ac. Tub. (Green) and EMA(Red) showing movement of EMA-stained vesicles on microtubules (F) In-vitro cultured untreated gonad and treated gonad (microtubule inhibitor Ciliobrevin D and cold treatment) stained for Ac. Tub (Green), EMA (Red) and DAPI (Blue). Quantification showing % germ cells with Mouse Fusome in Untreated versus Celiobrevin D/Cold treated E11.5 gonad. (Student's t-test: p-value **<0.01) (G) Lineage labelled 4-cell cyst stained at E12.5 for YFP (Green), EMA (Red) and Ac. Tub (Grey). (H) 3D modelling of lineage labelled cyst at E12.5. Video depicts animation video generated using Imaris software to create uniform spheres in green to position the cells within labelled 8-cell cyst (upper panel) and 10-cell cyst (lower panel) and surface rendering of EMA-stained fusome within lineage labelled germ cells. (H') YFP-labelled cells (green spots) and surface-rendered EMA (grey surface) using Imaris. Yellow Arrows pointing to fusome surface within nearest germ cell to the putative cleavage site (H") Quantification of fusome volume in the nearest germ cells to the putative cleavage sites. N=15 lineage labelled cyst with clear Ac. Tub connections were analyzed (Student's t-test, p-value *<0.05). Scale bar: 5 µm (A-B), 10 µm (C-F).

Fig. S3: Pard3 gene expression in E12.5-E13.5 gonad (A) Z-stack video of E12.5 gonad stained for EMA (Green), PARD3 (Red) and DAPI (Blue) (See Video S3A). (B) Z-stack video of E13.5 ovary **(**♀**,** See Video S3B1**)** and E13.5 testis **(**♂**,** See Video S3B2**)** stained for EMA (Green), PARD3 (Red) and GCNA (Blue). (C) Zoomed images of E13.5 gonad stained for RACGAP (Green) and Pard3 (Red) (D) E13.5 ovaries stained for GCNA (Blue), EMA (Green) and PARD3 (Red). (E) Lineage labelled E13.5 ovary stained for YFP (Green), GCNA (Blue), PARD3 (Red) and EMA (Grey). (F) Quinacrine (Male chromosome specific stain, Red) and DAPI (Green) staining of male vs female fetal tail samples (F) Feature plot and UMAP plot depicting Xist expression within E10.5 and E11.5 gonad followed by bioinformatic segregation of female gonadal germ cells (XX only) to avoid Quinacrine false-negative by segregating the cells expressing significant amount of XX specific genes (eg: Xist, Ddx3x, Utx) depicted in UMAP plot as XX only cells. (G) E10, E11 and E15 (10X genomics) scRNA seq was performed and germ cells isolated bioinformatically. Cluster of germ cells from E12, E14, E16, E18, P1 and P5 of previously published data (NCBI: Niu and Spradling, 2020) were used to create E10.5-P5 merged germ cell data to comprehensively look at gene expression across developmental stages. The number of cells used to create merged dataset is shown. (H) Feature plot validating that all the cells express germ cell specific markers (Dppa3/DDx4) in stage dependent manner (I) Pre-meiotic/Meiotic gene expression analysis depicted by feature plot for various developmental stages within merged dataset. (J) Stack violin plot depicting Golgi-UPR pathway associated gene expression pattern across E10.5 to P5 meiotic germ cell and nurse cell developmental stages. Scale bar= 20 µm (A,B-B) and 10 µm (C,D and F), 100 µm (E).

Fig. S4: Validation of female Dazl mutant phenotype, MACS and Activity assays. (A) Expected absence of Dazl protein in Dazl mutant gonad is shown by staining of E18.5 WT and Dazl-/- gonad for Dazl (Red), GCNA (Green) and DAPI (Grey). (B) E12.5 WT and Dazl$^{-/-}$ gonad stained for DNMT3a (Red), EMA (Green) and DAPI (Grey) (C) Fetal tail genotyping for scRNA sequencing: Gel electrophoresis showing the standard *Dazl* genotyping PCR assay by Jackson (Stock No: 035880 Protocol 40585) with expected results: Wild type (192 bp), Heterozygous mutant (300 and 192 bp) and Homozygous mutant (300 bp). (D) Feature plot depicting positive Xist Expression in scRNA seq data of E11.5 and E12.5 Dazl mutant fetal gonad, thus concluding them as female samples. (E) Stackviolin Plot depicting pluripotency gene expression pattern in

E11.5-E12.5 WT vs Dazl-/- gonad. (F) Stackviolin Plot depicting Xbp1 targets gene and Drosophila fusome ortholog gene expression pattern in E11.5 WT vs Dazl-/- gonad (G) Staining of both unbound SSEA1(-ve) and the bound fraction consisting of SSEA1(+ve) cells for DDX4 (Magenta) and DAPI (Grey). (H) Gel electrophoresis showing the PCR amplification of housekeeping gene GAPDH and Germ cell specific marker DDX4 in SSEA1(-ve) and SSEA1 (+ve) germ cells from E11.5 and E12.5 ovary. The amplicon size is indicated on left. (I) Proof of functioning of Xbp1 assay is shown by staining of both mixture of SSEA1(-ve) and SSEA1(+ve) cells for GCNA (Green), DAPI (Grey) and Xbp1(Red) (J) Proof of function of proteasome activity assay using Trypsin as technical positive control. The proteasome activity assay was shown for two different assays (I and II) with technical duplicates at three different Trypsin concentrations. Mean fluorescent intensity in arbitrary units is shown obtained using plate reader. Scale bar: 20 µm (A), 10 µm (B), 100 µm (G and I).

Fig. S5: Fusome enrichment within destined medullary Oocytes in WT vs Dazl mutant. (A-B) Zoomed out E17.5 ovary covering large span of tissue stained with DAPI (Blue), WGA (Red), GCNA (Green) and Tex14 (Yellow). White dotted line is zoomed in and shown separately in main figure (Refer to main Fig 5A and A'). (C) Video created using Imari software showing E17.5 ovary stained for GCNA (Green), Tex14 (Yellow) and WGA (Red) followed by surface rendering of WGA aggregate (continuous one) associated with ring canals. (See Video S5C) (D) Video of E18.5 female gonad stained with DAPI (Blue), GCNA (Green) and WGA (Red) depicts the cortex and medullary region where medullary region showing distinct enriched WGA aggregate compared to surrounding small nurse cells. (See Video S5D) (D') One of the z-stack form E18.5 ovary Video in E stained with DAPI, GCNA and WGA depicts the medullary big Oocyte-like cells showing distinct enriched WGA aggregate compared to surrounding small nurse cells. E) Z-stack video of E18.5 WT, Dazl +/- and Dazl-/- gonad stained for GCNA (Green) and WGA (Red). (See Videos S5E1 to S5E3). (F) Z-stack video of P0 WT, Dazl +/- and Dazl-/- gonad stained for GCNA(Green) and PARD3 (Red). (See S5 F1 to F3) (G) E18.5 WT and Dazl +/- gonad stained for Mitotracker (Red) and GCNA (Green). Scale bar: 20 µm (A-B and G), 50 µm (D-E), 100 µm (F).

Fig 1.

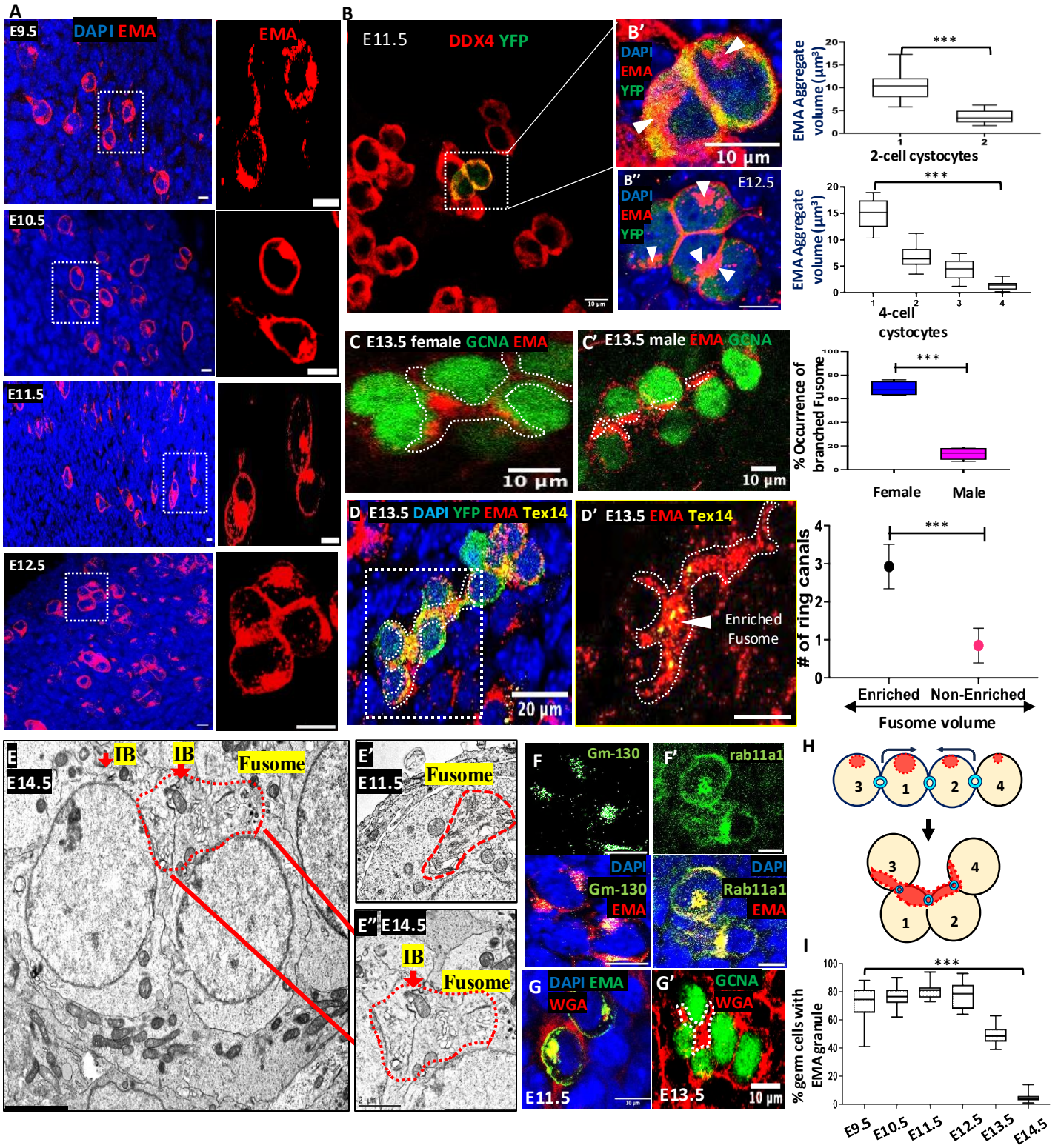
A
E9.5
DAPI EMA
EMA
E10.5
E11.5
E12.5
B
E11.5
DDX4 YFP
B'
DAPI
EMA
YFP
10 µm
B''
E12.5
DAPI
EMA
YFP
EMA Aggregate volume (µm³)
***
2-cell cystocytes
4-cell cystocytes
C E13.5 female GCNA EMA
C' E13.5 male EMA GCNA
10 µm
% Occurrence of branched Fusome
Female
Male
D E13.5 DAPI YFP EMA Tex14
D' E13.5 EMA Tex14
Enriched Fusome
20 µm
# of ring canals
Enriched
Non-Enriched
Fusome volume
E
E14.5
IB
IB
Fusome
E'
E11.5
Fusome
E''
E14.5
IB
Fusome
F
Gm-130
F'
rab11a1
DAPI
Gm-130
EMA
DAPI
Rab11a1
EMA
G
DAPI EMA
WGA
E11.5
G'
GCNA
WGA
E13.5
10 µm
H
3
1
2
4
I
% germ cells with EMA granule
E9.5
E10.5
E11.5
E12.5
E13.5
E14.5

Fig 2.

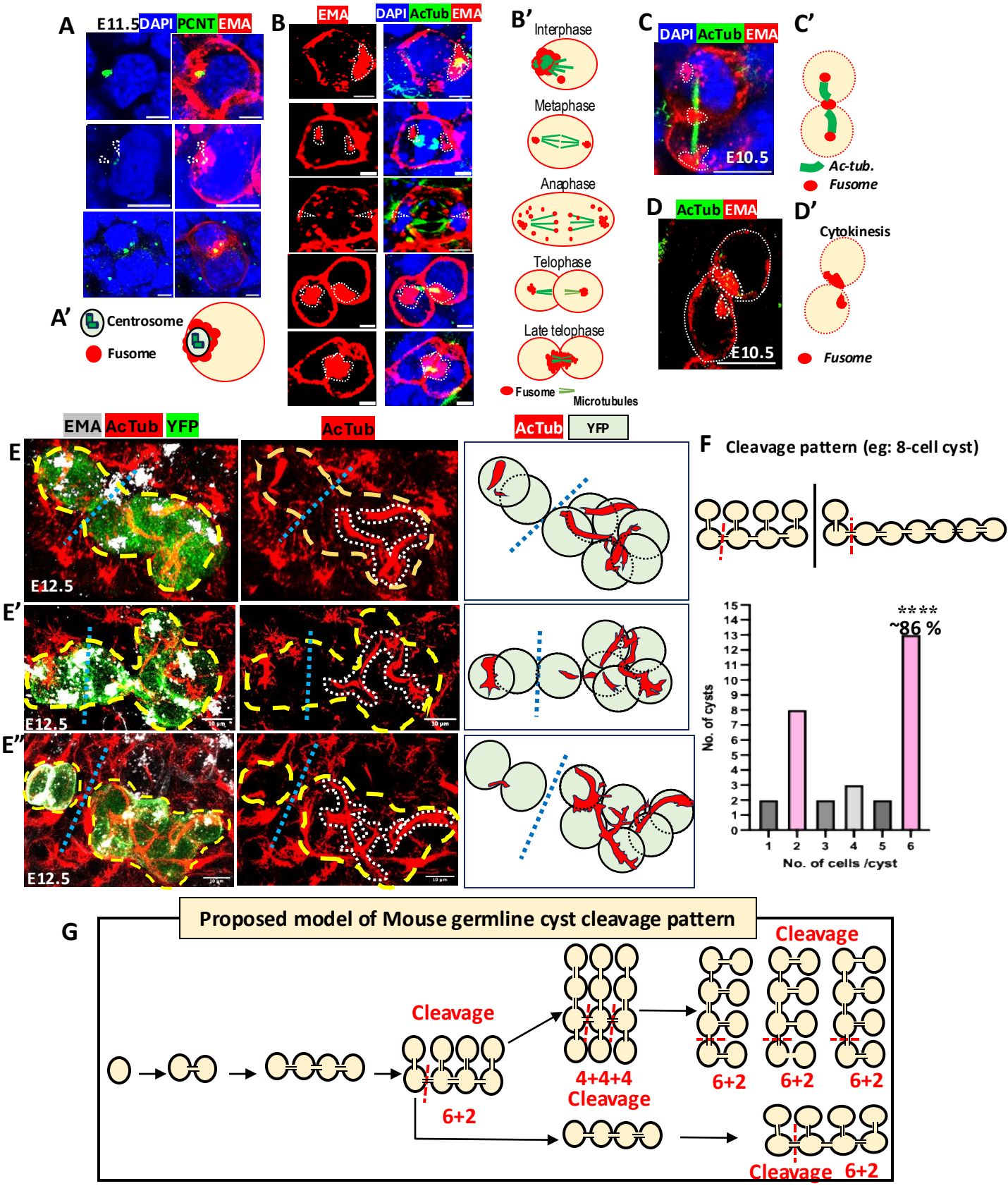
A
E11.5
DAPI
PCNT
EMA
A'
Centrosome
Fusome
B
EMA
DAPI
AcTub
EMA
B'
Interphase
Metaphase
Anaphase
Telophase
Late telophase
Fusome
Microtubules
C
DAPI
AcTub
EMA
E10.5
C'
Ac-tub.
Fusome
D
AcTub
EMA
E10.5
D'
Cytokinesis
Fusome
EMA
AcTub
YFP
AcTub
AcTub
YFP
E
E12.5
E'
E12.5
E''
E12.5
F
Cleavage pattern (eg: 8-cell cyst)
No. of cysts
No. of cells /cyst
****
~86 %
G
Proposed model of Mouse germline cyst cleavage pattern
Cleavage
6+2
4+4+4
Cleavage
6+2
Cleavage
6+2
6+2
Cleavage
6+2

Fig 3.

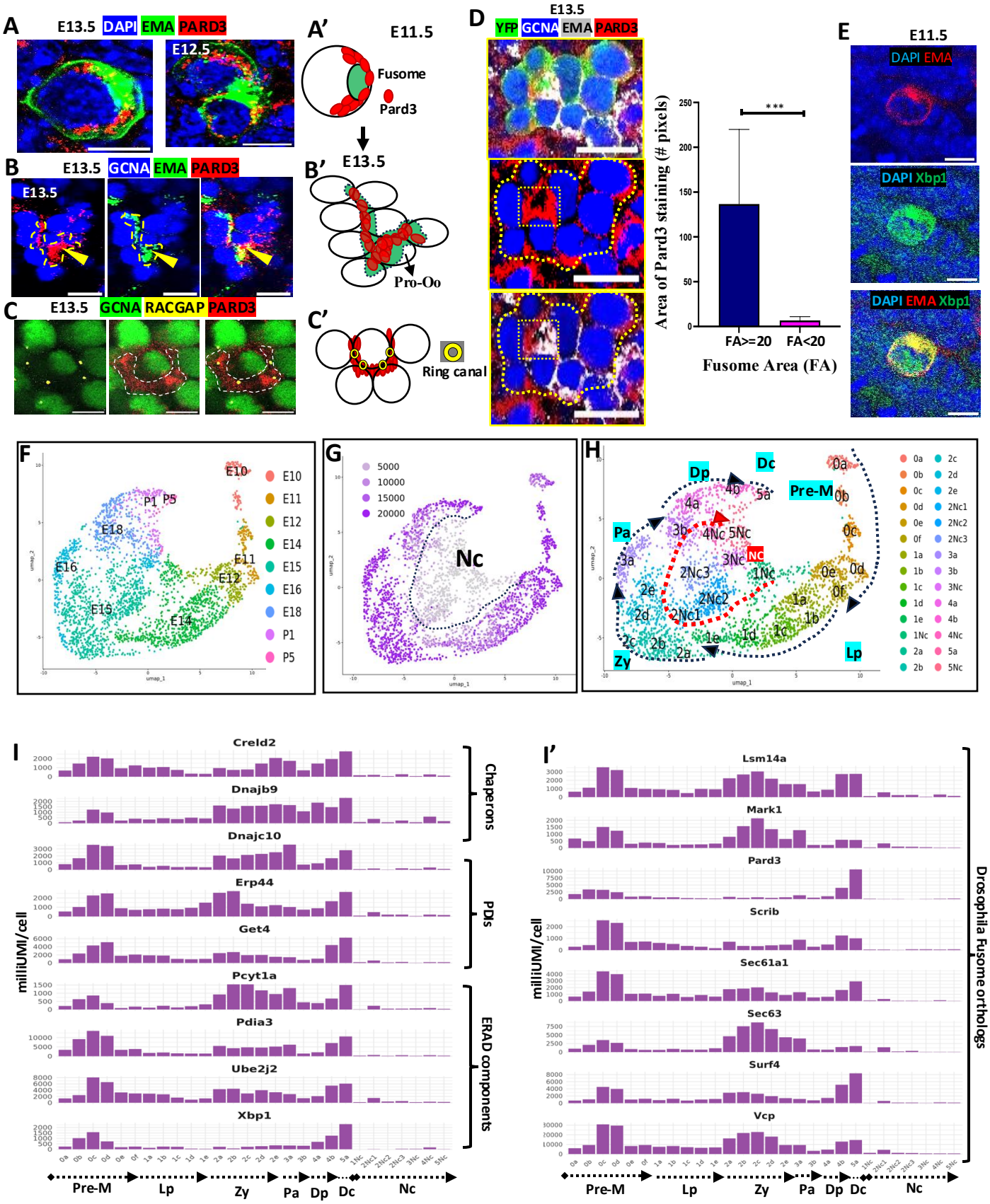
A
E13.5 DAPI EMA PARD3
E12.5
A'
E11.5
Fusome
Pard3
B
E13.5 GCNA EMA PARD3
E13.5
B'
E13.5
Pro-Oo
C
E13.5 GCNA RACGAP PARD3
C'
Ring canal
D
E13.5
YFP GCNA EMA PARD3
Area of Pard3 staining (# pixels)
***
FA>=20
FA<20
Fusome Area (FA)
E
E11.5
DAPI EMA
DAPI Xbp1
DAPI EMA Xbp1
F
E10
E11
E12
E14
E15
E16
E18
P1
P5
G
5000
10000
15000
20000
Nc
H
Dp
Dc
Pre-M
Pa
Nc
Zy
Lp
I
Creld2
Dnajb9
Dnajc10
Erp44
Get4
Pcyt1a
Pdia3
Ube2j2
Xbp1
milliUMI/cell
Chaperons
PDIs
ERAD components
Pre-M
Lp
Zy
Pa
Dp
Dc
Nc
I'
Lsm14a
Mark1
Pard3
Scrib
Sec61a1
Sec63
Surf4
Vcp
Drosophila Fusome orthologs

Fig 4.

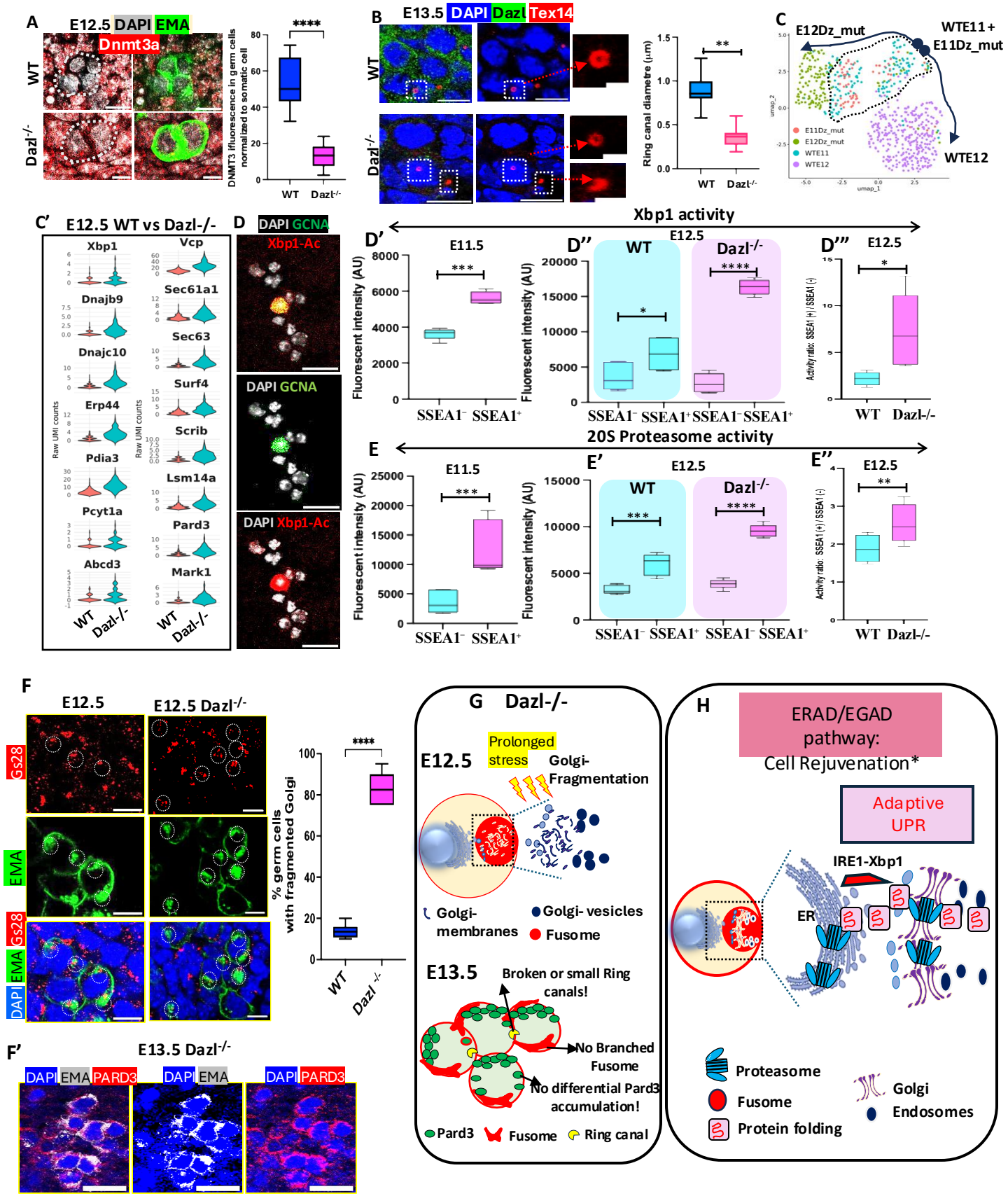
A
E12.5 DAPI EMA
Dnmt3a
WT
Dazl-/-
DNMT3 ifluorescence in germ cells normalized to somatic cell
****
WT
Dazl-/-
B
E13.5 DAPI Dazl Tex14
WT
Dazl-/-
Ring canal diametre (µm)
**
WT
Dazl-/-
C
E12Dz_mut
WTE11 + E11Dz_mut
WTE12
E11Dz_mut
E12Dz_mut
WTE11
WTE12
umap_1
umap_2
C'
E12.5 WT vs Dazl-/-
Xbp1
Vcp
Dnajb9
Sec61a1
Sec63
Dnajc10
Surf4
Erp44
Scrib
Pdia3
Lsm14a
Pcyt1a
Pard3
Abcd3
Mark1
Raw UMI counts
WT
Dazl-/-
D
DAPI GCNA
Xbp1-Ac
DAPI GCNA
DAPI Xbp1-Ac
Xbp1 activity
D'
E11.5
***
Fluorescent intensity (AU)
SSEA1⁻ SSEA1⁺
D''
E12.5
WT
Dazl-/-
*
****
SSEA1⁻ SSEA1⁺ SSEA1⁻ SSEA1⁺
D'''
E12.5
*
Activity ratio: SSEA1 (+) / SSEA1 (-)
WT Dazl-/-
20S Proteasome activity
E
E11.5
***
SSEA1⁻ SSEA1⁺
E'
E12.5
WT
Dazl-/-
***
****
SSEA1⁻ SSEA1⁺ SSEA1⁻ SSEA1⁺
E''
E12.5
**
WT Dazl-/-
F
E12.5
E12.5 Dazl-/-
Gs28
EMA
Gs28
EMA
DAPI
% germ cells with fragmented Golgi
****
WT
Dazl-/-
F'
E13.5 Dazl-/-
DAPI EMA PARD3
DAPI EMA
DAPI PARD3
G
Dazl-/-
E12.5
Prolonged stress
Golgi-Fragmentation
Golgi-membranes
Golgi- vesicles
Fusome
E13.5
Broken or small Ring canals!
No Branched Fusome
No differential Pard3 accumulation!
Pard3
Fusome
Ring canal
H
ERAD/EGAD pathway:
Cell Rejuvenation*
Adaptive UPR
IRE1-Xbp1
ER
Proteasome
Fusome
Protein folding
Golgi
Endosomes

Fig 5.

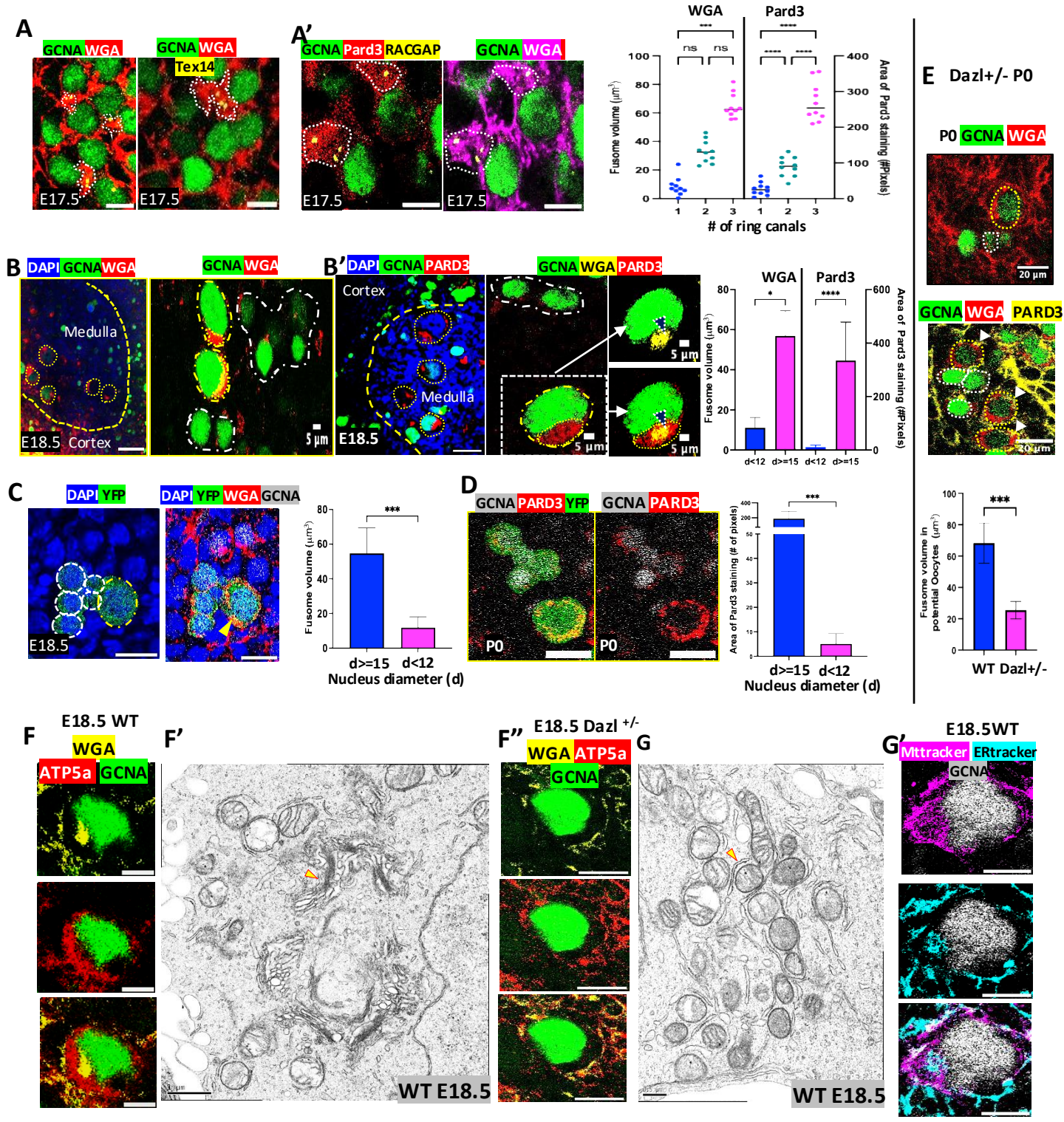
A
GCNA WGA
E17.5
GCNA WGA Tex14
E17.5
A'
GCNA Pard3 RACGAP
E17.5
GCNA WGA
E17.5
WGA
Pard3
ns
ns
Fusome volume (µm³)
Area of Pard3 staining (#Pixels)
# of ring canals
E Dazl+/- P0
P0 GCNA WGA
20 µm
GCNA WGA PARD3
20 µm
B DAPI GCNA WGA
Medulla
E18.5 Cortex
GCNA WGA
5 µm
B' DAPI GCNA PARD3
Cortex
Medulla
E18.5
GCNA WGA PARD3
5 µm
5 µm
5 µm
WGA
Pard3
Fusome volume (µm³)
Area of Pard3 staining (#Pixels)
d<12 d>=15 d<12 d>=15
C DAPI YFP
E18.5
DAPI YFP WGA GCNA
Fusome volume (µm³)
d>=15 d<12
Nucleus diameter (d)
D GCNA PARD3 YFP
P0
GCNA PARD3
P0
Area of Pard3 staining (# of pixels)
d>=15 d<12
Nucleus diameter (d)
Fusome volume in potential Oocytes (µm³)
WT Dazl+/-
F E18.5 WT
WGA
ATP5a GCNA
F'
WT E18.5
F'' E18.5 Dazl +/-
WGA ATP5a
GCNA
G
WT E18.5
G' E18.5WT
Mttracker ERtracker
GCNA